Journal of Earth Science, *Vol. xx*, *No. x*, *p. xxx–xxx*, *online 2021* *ISSN 1674-487X*
Printed in China
https://doi.org/10.1007/s12583-020-1389-4

Magmatic Evolution of Garnet-Bearing Highly Fractionated Granitic Rocks from Macao, Southeast China: Implications for Granite-Related Mineralization Processes

Pedro Quelhas[1, 2], **João Mata**[2], **Ágata Alveirinho Dias**[*1, 2]
1. *Institute of Science and Environment*, *University of Saint Joseph*, *Rua de Londres*, 106 *Macao*, *China*
2. *Instituto Dom Luiz*, *Faculdade de Ciências*, *Universidade de Lisboa*, 1749-016 *Lisboa*, *Portugal*
Pedro Quelhas: https://orcid.org/0000-0001-9481-8660; Ágata Alveirinho Dias: https://orcid.org/0000-0003-3026-7366

ABSTRACT: The widespread W-(Mo)-Sn-Nb-Ta polymetallic mineralization in Southeast (SE) China is genetically associated with Mesozoic highly fractionated granitic rocks. Such rocks have enigmatic mineralogical and geochemical features, making its petrogenesis an intensely debated topic. To better understand the underlying magma evolution processes, petrography, garnet chemistry and whole-rock major and trace element data are reported for Jurassic highly fractionated granitic rocks and associated microgranite and aplite-pegmatite dikes from Macao and compared with coeval similar granitic rocks from nearby areas in SE China. Despite the fact that the most evolved rocks in Macao are garnet-bearing aplite-pegmatite dikes, the existence of coeval two-mica and garnet-bearing biotite and muscovite granites displaying more evolved compositions (e.g., lower Zr/Hf ratios) indicates that the differentiation sequence reached higher degrees of fractionation at a regional scale. Although crystal fractionation played an important role, late-stage fluid/melt interactions, involving F-rich fluids, imparted specific geochemical characteristics to Macao and SE China highly fractionated granitic rocks such as the non-CHARAC (CHArge-and-RAdius-Controlled) behavior of trace elements, leading, for example, to non-chondritic Zr/Hf ratios, Rare Earth Elements (REE) tetrad effects and Nb-Ta enrichment and fractionation. Such process contributed to the late-stage crystallization of accessory phases only found in these highly evolved facies. Among the latter, two populations of garnet were identified in MGI (Macao Group I) highly fractionated granitic rocks: small grossular-poor euhedral grains and large grossular-rich skeletal garnet grains with quartz inclusions. The first group was mainly formed through precipitation from highly evolved Mn-rich slightly peraluminous melts under low-pressure and relatively low temperature (~700 ºC) conditions. Assimilation of upper crust metasedimentary materials may have contributed as a source of Mn and Al to the formation of garnet. The second group has a metasomatic origin related to the interaction of magmatic fluids with previously crystallized mineral phases and, possibly, with assimilated metasedimentary enclaves or surrounding metasedimentary strata. The highly fractionated granitic rocks in Macao represent the first stage in the development of granite-related W-(Mo)-Sn-Nb-Ta mineralization associated with coeval more evolved lithotypes in SE China.
KEY WORDS: highly fractionated granites, aplite, Macao (South China), Jurassic, late-stage fluid/melt interactions, garnet, non-CHARAC, REE tetrad effect.

0 INTRODUCTION

From genesis to emplacement, granitic magmas can undergo significant degrees of differentiation leading to the formation of highly fractionated rocks such as fine-grained granites, aplites and pegmatites (Wu et al., 2017; London and Kontak, 2012; Neiva and Ramos, 2010; Simmons and Webber, 2008; Neiva et al., 2008). Aplites and pegmatites usually occur as segregations along the margins of cupolas of granitic plutons and/or sharply discordant dikes intruding igneous and metamorphic rocks (London, 2014; London and Kontak, 2012). Such highly evolved rocks are characterized by compositions close to the granite system minimum or eutectic (London et al., 2012; Jahns and Tuttle, 1963; Tuttle and Bowen, 1958), which confer them an utmost importance in the assessment of processes occurring during the latest stages of granitic magmas differentiation (Dill, 2015; London, 2008). Since pegmatites have an extremely coarse but variable grain-size, it is often difficult to obtain representative whole-rock chemical analyzes. Considering this, and the fact that aplites are compositionally similar to pegmatites for most, but volatile, elements (Dill, 2015), studies on the late stages of differentiation of granitic magmas often rely on the geochemistry of aplitic facies (e.g., Antunes et al., 2013; Neiva et al., 2012, 2008).

*Corresponding author: agata.dias@usj.edu.mo

Manuscript received July 7, 2020.
Manuscript accepted December 4, 2020.

Quelhas, P., Mata, J., Dias, Á. A., 2021. Magmatic Evolution of Garnet-Bearing Highly Fractionated Granitic Rocks from Macao, Southeast China: Implications for Granite-Related Mineralization Processes. *Journal of Earth Science*, xx(x): xxx–xxx. https://doi.org/10.1007/s12583-020-1389-4. http://en.earth-science.net

In general, granitic magmas contain water between 3 wt.% to 6 wt.% and the partial pressures of magmatic gases can achieve several hundred bars (Lowenstern, 1994). As crystallization proceeds, the vapor pressure increases and the hydrostatic head of the magma may be exceeded, producing a separate vapor/fluid phase at the late stages of magmatic evolution (Chen and Grapes, 2007). At this stage, large amounts of the vapor/fluid phase can mobilize and remove significant quantities of chemical elements from high-silica magmas to other locations (inside and/or outside of the pluton), leaving marked effects on the chemical composition of the residual magma (e.g., Monecke et al., 2007; Wu et al., 2004; Monecke et al., 2002; Jahn et al., 2001; Irber, 1999; Bau, 1996; Clarke, 1992; Masuda et al., 1987). On the other hand, increasing contents of fluxing agents (H_2O, Li, B, F, P, and/or Cl; Bau, 1997, 1996; London, 1992) significantly reduce the viscosity and solidus temperature of the magma, promoting concentration of rare or large-ion lithophile elements (LILE) in the residual melt, which results in crystallization of several mineral phases not found in less evolved rocks (e.g., topaz, phosphates, lithium micas, tourmaline, cassiterite, Mn-rich garnet, columbite-tantalite, microlite; Dill, 2015; Neiva et al., 2012). In addition, they also directly or indirectly contribute to a lower nucleation rate and higher crystal growth rates, causing the formation of pegmatitic textures (Nabelek et al., 2010).

The Mesozoic geology of the Cathaysia Block is characterized by widespread granitic rocks (Fig. 1), which are closely associated with large-scale polymetallic mineralization (Mao et al., 2013; Zhou et al., 2006). Highly evolved Jurassic granites are common and tend to occur as small stocks hosting different kinds of mineralization (Mo, W, Sn, U, REE, Nb-Ta, Cu, Pb and Zn; e.g., Cao et al., 2018; Jiang H. et al., 2018; Jiang W. et al., 2018; Wu et al., 2017; Xiang et al., 2017; Qiu et al., 2016; Zhou et al., 2016; Xu et al., 2015; Zhao et al., 2002). Despite the inherent economic potential that has prompted numerous and significant studies of granites, their origin and evolution, as well as the controlling factors of their distinct geochemistry and mineralogy, are still enigmatic. This is particularly true for the Pearl River Delta region in southern Guangdong Province (Southeast China), where Macao is located.

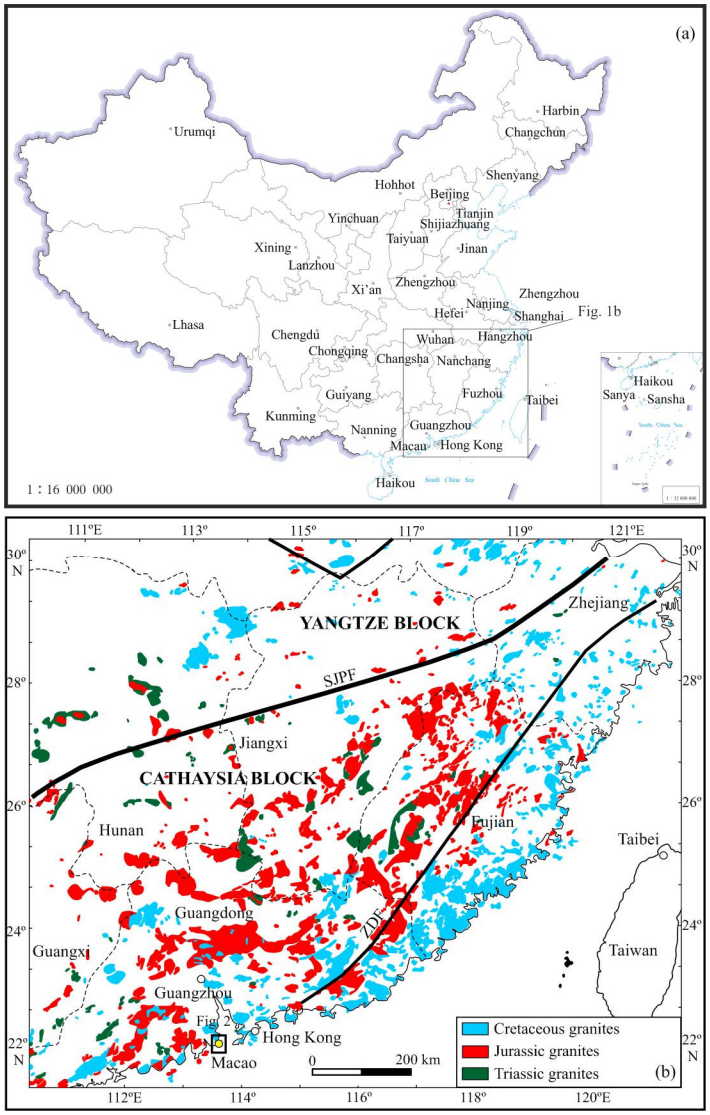

Figure 1. (a) Map of China showing the location of the studied region (GS(2019)1686); (b) geological map of SE China showing the distribution of Mesozoic granitic rocks (modified after Yang et al., 2018; Zhou et al., 2006). SJPF. Shaoxing-Jiangshan-Pingxiang fault; ZDF. Zhenghe-Dapu fault zone.

This study deals with the petrography, mineralogy and geochemistry of highly evolved fine- to medium-grained non-porphyritic granitic facies and aplites from Macao, in order to understand the dynamics of highly evolved granitic systems in this area of SE China. The magmatic evolution stage at which pegmatites were formed will be interpreted in the light of the geochemistry of aplite and microgranite dikes. The objectives are: (1) to understand the relationship between highly fractionated granites and the aplite-pegmatite dikes; (2) to identify and describe the evolution processes responsible for the mineralogical and geochemical characteristics of these rocks; (3) to assess the role of fluids on the late-stage evolution of granitic magmas; (4) to unravel the origin of garnet occurring in the highly evolved granitic rocks in Macao and; (5) to establish the relationship between these rocks and the wide spread highly fractionated, and often mineralized, Jurassic granites in SE China. To achieve these, petrography, mineral chemistry and whole-rock elemental geochemical data are presented and discussed in this paper.

1 GEOLOGICAL SETTING

The territory of Macao is part of the Cathaysia Block, which, during the Early Neoproterozoic, amalgamated to the Yangtze Block in the northwest, along the Jiangshan-Shaoxing suture zone, forming the South China Block (SCB; e.g., Charvet, 2013; Wang et al., 2013; Ye et al., 2007; Li et al., 2002). Macao is located in southern Guangdong Province, along the coast of SE China, ca. 50 km to the west of Hong Kong, on the western margin of the Pearl River Delta. In this region, there is a predominance of granitic intrusions belonging to the ~3 500 km long and ~800 km wide NE-trending Mesozoic Southeast China Magmatic Belt (Fig. 1; Zhou et al., 2006). Jurassic to Cretaceous granitoids, in particular, were formed due to intense magmatic activity during the Yanshanian Orogeny, which is thought to be related to the subduction of the Paleo-Pacific plate under the Eurasian plate (e.g., Quelhas et al., 2021; Wang et al., 2013; Jiang et al., 2009; Li and Li, 2007; Li et al., 2007; Zhou et al., 2006; Zhou and Li, 2000).

The Mesozoic volcanic-plutonic rocks intruded Late Paleozoic and younger Early to Middle Jurassic sedimentary successions deformed and metamorphosed by several tectonic events (Quelhas et al., 2021; Huang et al., 2013; Sewell et al., 2000; Ribeiro et al., 1992; Sewell et al., 1992). To the west of Macao, along the southern coastal region of the Guangdong Province, a few Late Jurassic amphibole-bearing granites occur as stocks/small plutons (Huang et al., 2013). However, most of the granites in the region form larger plutons or batholiths composed of biotite granites (rarely containing amphibole) spatially associated with volumetrically minor tourmaline-, muscovite- and garnet-bearing granites, mainly emplaced between 166–155 Ma (Quelhas et al. 2020; Huang et al. 2013).

Several studies have contributed to the knowledge on the geology of Macao for the past few decades (Quelhas et al., 2021, 2020; Ribeiro et al., 2010, 1992; Carrington da Costa and Lemos, 1964; Costa, 1944; Neiva, 1944). The territory (~30 km²) is composed by several granitic intrusions belonging to a Jurassic batholith extending about 50 km to the north, which intrudes Paleozoic sedimentary strata (Huang et al., 2013; Quelhas et al., 2021; Ribeiro et al., 1992). Remnants of the wall-rock are present as metasedimentary enclaves of Devonian age enclosed within the granites (Quelhas et al., 2021). The dominant lithology is biotite granite, with minor Microgranular Mafic Enclaves (MME), that is intruded by a relatively diversified swarm of granitic and quartz dikes (and veins) and by younger Middle Jurassic to Cretaceous dacite dikes (Fig. 2). The granitic rocks consist of two chemically and age distinct groups of I-type granites: Macao Group I (MGI; 164.5±0.6 to 162.9±0.7 Ma) and Macao Group II (MGII; 156.6±0.2 to 155.5±0.8 Ma) granites (Quelhas et al. 2020). It has been proposed that these granitic magmas were generated by partial melting of infracrustal medium- to high-K basaltic Paleoproterozoic to Mesoproterozoic protoliths, though each group had a different magmatic evolution history (Quelhas et al., 2021). Each group, in its turn, can be subdivided in "weakly to moderately fractionated granites" (Zr/Hf>25) and "highly fractionated granites" (Zr/Hf≤25; Quelhas et al., 2021, 2020). This study will focus on the MGI highly fractionated granitic rocks, including the associated microgranite, aplite and pegmatite dikes. The MGI highly fractionated granites (Figs. 3b–3f) either occur as large bodies of medium- to coarse-grained non-porphyritic biotite granites gradually changing into less fractionated coarse-grained porphyritic varieties or as small stocks of fine-grained granites in the margins of the main granitic intrusions (Fig. 2). In the latter case, aplites and pegmatites tend to be particularly abundant, occurring either as sharply discordant dikes (Fig. 3j) or as segregations within the highly fractionated granites (Fig. 3i). The contacts between aplite-pegmatite dikes and the host granites vary between straight and irregular sharp to gradual. The microgranite dikes tend to be larger (decimeter to meter-wide) than the aplite dikes, have sharp contacts with the host granite and their texture is uniform (Fig. 3g). The aplites, on the other hand, occur as smaller dikes (centimeter to decimeter-wide), with typical sugary texture and often show gradual variation in grain size to pegmatitic textures (Fig. 3j).

2 METHODOLOGIES

2.1 Mineral Chemistry

Mineral analyses were performed on carbon-coated polished thin sections using a JEOL SUPERPROBE™, model JXA-8200, in wavelength dispersive mode at the Departamento de Geologia da Faculdade de Ciências da Universidade de Lisboa (Portugal). Minerals were analyzed with an acceleration voltage of 15 kV and a current of 25 nA, using a 5 μm wide beam. The analyses were calibrated using the composition of in-house standard materials, with reproducibility errors being lower than 2% and ordinarily around 1%. Matrix effects were corrected using the ZAF software provided by JEOL. Information about standards and detection limits are given in Supplementary File 1a.

2.2 Whole-Rock Elemental Geochemistry

Whole-rock major and trace element concentrations were obtained at Activation Laboratories, Ltd. (Ancaster, Ontario, Canada) using the geochemical analytical package 4E-Research. Major oxide content was analyzed using Inductively Coupled Plasma-Optical Emission Spectrometry (ICP-OES) using a Thermo Jarrell-Ash ENVIRO II ICP and/or Spectro Cirros

ICP. Trace elements, including Rare Earth Elements (REE), were obtained using Inductively Coupled Plasma Mass-Spectrometry (ICP-MS) on a Perkin Elmer SCIEX ELAN 6000, 6100 or 9000 ICP/MS and by Instrumental Neutron Activation Analysis (INAA). In-house standards and several certified reference materials of granitic to dioritic compositions (s.l.) from USGS (United States Geological Survey), GSJ (Geological Survey of Japan) and CCRMP (Canadian Certificate Reference Material Project) were used. Errors associated with the accuracy are ≤4% for major elements and better than 9% for the REE and the most widely used incompatible elements. Duplicate measurements of samples indicate that errors associated with reproducibility were generally lower than 5% for both major and trace elements. Information about detection limits is given in Supplementary File 1B. For detailed information regarding analytical and control procedures consult the Actlabs website (www.actlabs.com).

3 RESULTS

3.1 Petrography

The petrographic and mineralogical features of Macao granites have been described in previous studies (Quelhas et al., 2021, 2020). Here we focus more specifically, and with more detail, on the mineralogy and textures of MGI highly fractionated granitic rocks, including microgranites and aplite-pegmatites.

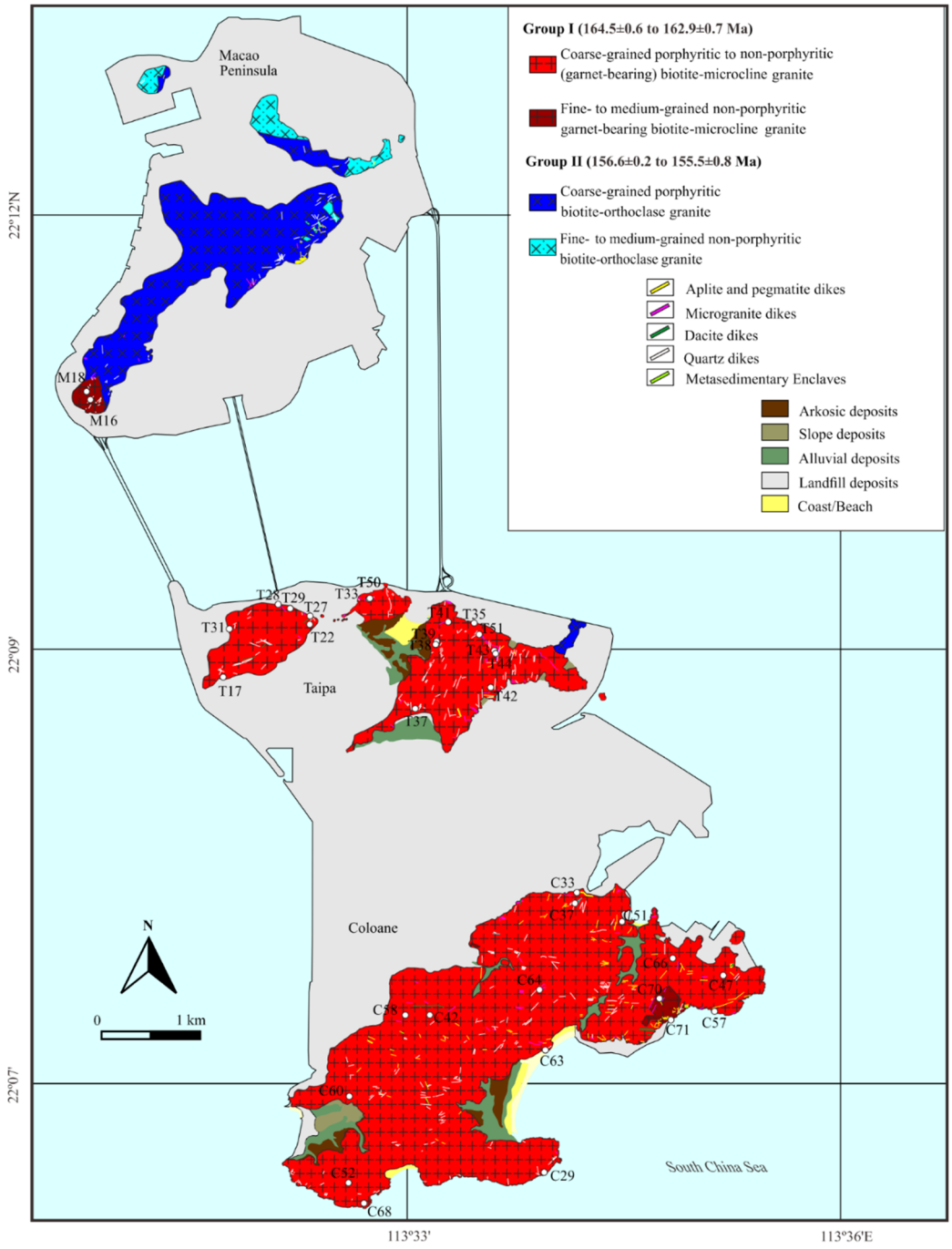

Figure 2. Simplified geological map of Macao showing the distribution of the two groups of granitic rocks and the location of samples analyzed in this study (modified after Quelhas et al., 2021, 2020).

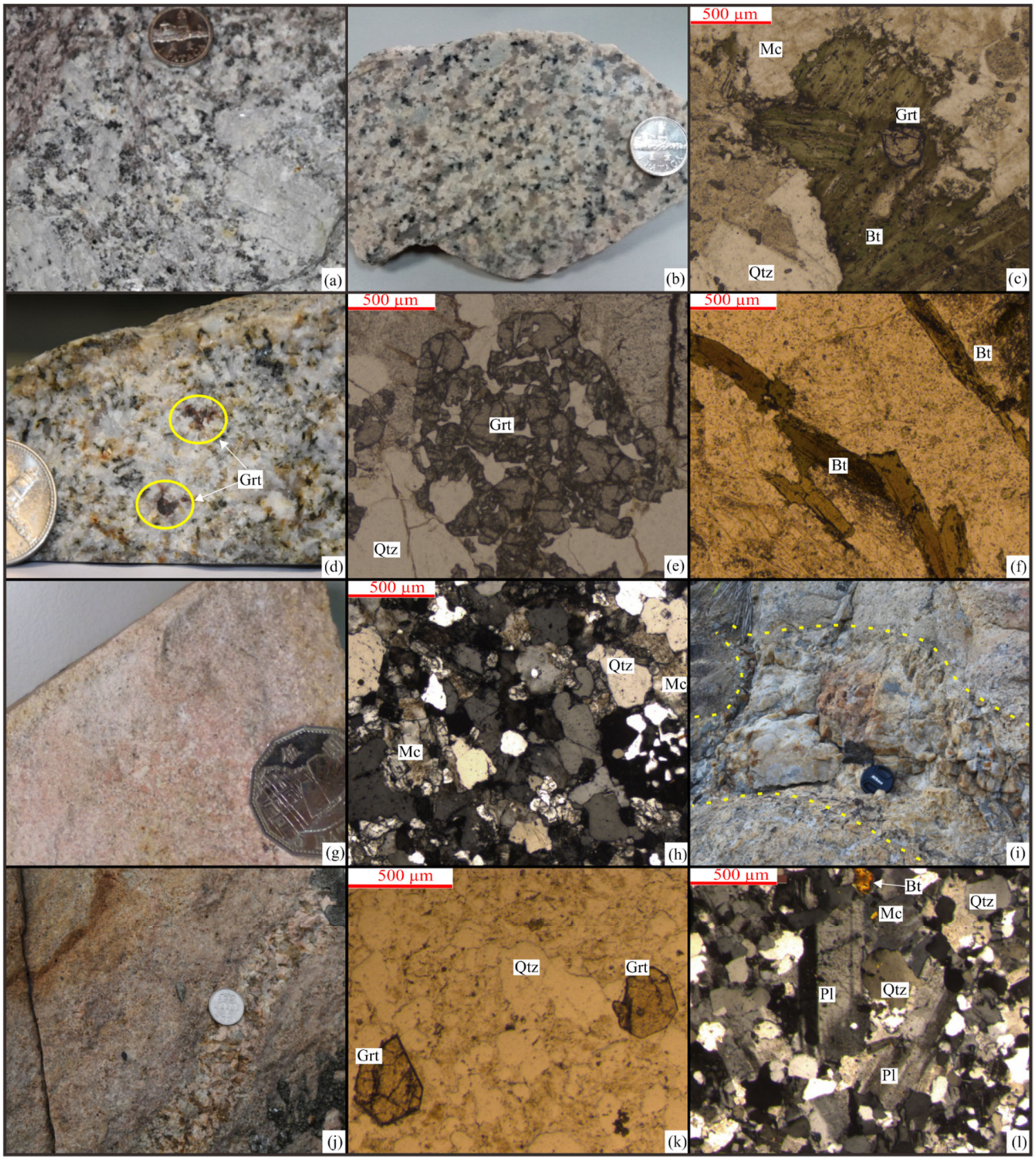

Figure 3. Representative hand specimens and thin-sections of the Macao Group I (MGI) weakly to moderately fractionated (a) and highly fractionated (b)–(l) granitic rocks: (a) large microcline megacrysts in a coarse-grained porphyritic biotite granite; (b) medium- to coarse-grained non-porphyritic garnet-bearing biotite granite; (c) garnet associated with biotite in a medium- to coarse-grained non-porphyritic garnet-bearing biotite granite; (d) fine- to medium-grained non-porphyritic garnet-bearing biotite granite, with two crystals of red-brownish garnet; (e) garnet-quartz intergrowth in a fine- to medium-grained non-porphyritic garnet-bearing biotite granite; (f) lath-shaped biotite crystals in a fine- to medium-grained non-porphyritic garnet-bearing biotite granite; (g) fine-grained equigranular microgranite dike; (h) microcline and quartz anhedral grains and graphic texture in a microgranite dike; (i) pod-shaped pegmatite associated with a fine- to medium-grained non-porphyritic garnet-bearing biotite granite; (j) aplite-pegmatite dike with the pegmatite in the center surrounded by aplite; (k) two euhedral garnet grains in an aplite dike; (l) microtexture of the aplite dike, showing subhedral tabular plagioclase and anhedral quartz and K-feldspar grains. Qtz. quartz; Pl. plagioclase; Mc. microcline; Bt. biotite; Grt. garnet.

The MGI weakly to moderately fractionated facies have a strong porphyritic character (Fig. 3a) in contrast with the MGI highly fractionated granites, which mainly occur as coarse-to medium-grained non-porphyritic garnet-bearing biotite-

microcline facies (Figs. 3b, 3c) gradually changing into slightly porphyritic facies in Taipa (Fig. 2). The MGI highly fractionated granites also occur as small intrusions of fine-to medium-grained non-porphyritic garnet-bearing biotite-microcline granite (Figs. 3d–3f) in Macao Peninsula and Coloane (Fig. 2). Under the microscope, the texture is xenomorphic. Alkali feldspar is present as anhedral to subhedral tabular perthite grains (<2 cm), showing Carlsbad twinning and weak undulatory extinction. Sodic feldspar blebs are usually weakly developed, with irregular contours, rarely showing polysynthetic twins. It is often poikilitic, including fine crystals of anhedral quartz and subhedral tabular zoned plagioclase. Plagioclase is less abundant than alkali feldspar, occurring as anhedral to subhedral tabular weakly sericitized grains (<1 cm), with polysynthetic twinning (rarely combined with Carlsbad twins) and occasionally showing continuous normal zoning. Quartz grains are inequigranular and anhedral (<1 cm; Fig. 3e), with irregular to sutured boundaries and strong undulatory extinction. The grains are frequently fractured and sub-granulated. Biotite occurs as aggregates of subhedral plates in coarse-grained facies (Fig. 3c) and as subhedral elongated lath-shaped crystals in fine-grained facies (Fig. 3f), pleochroic between pale yellow and green and moderately chloritized. Some crystals have abundant pleochroic haloes surrounding inclusions of zircon, monazite, xenotime and thorite. In coarse-grained facies, garnet occurs as small light brown subhedral crystals (<0.5 mm; Fig. 3c) associated with biotite, whereas in fine-grained facies it occurs as light brown anhedral to subhedral large skeletal crystals (<5 mm; Figs. 3d, 3e), forming symplectitic intergrowths with quartz. Other accessory minerals include: ilmenite, magnetite, fluorite, apatite, allanite, thorite, fergusonite, gadolinite, columbite-tantalite and sulfides.

Microgranite dikes tend to be more abundant in some specific areas (e.g., northeastern areas of Taipa main intrusions; Fig. 2) and display a wide range of widths (from centimeter to meter-wide). These rocks are leucocratic (in some cases slightly pinkish due to K-feldspar alteration; Fig. 3g) and have a fine-grained (<0.1 cm), moderately equigranular xenomorphic texture (Figs. 3g, 3h). Alkali feldspar is represented by fine-grained anhedral microperthite with weak undulatory extinction (Fig. 3h) and, in some cases, with poikilitic texture, hosting inclusions of quartz and plagioclase. Sodic blebs are rarely well-developed to the point of showing polysynthetic twinning. Plagioclase is less abundant than alkali feldspar, occurring as fine-grained subhedral tabular crystals with polysynthetic twinning. Quartz is present as fine-grained intergranular anhedral grains with undulatory extinction and as worm-like intergrowths with alkali feldspar, producing abundant graphic textures (Fig. 3h). Biotite is present as rare green to light yellow pleochroic fine-grained anhedral to subhedral flakes. The flakes are weakly to strongly chloritized and often show deformation features such as broken crystals and bent cleavages. Garnet occurs as light brown euhedral to subhedral isolated hexagonal and/or dodecahedron-shaped crystals (<500 μm), in textural equilibrium with surrounding minerals. Other accessory minerals include: Fe-Ti oxides, sulfides and fluorite.

Pegmatites occur essentially as dikes cutting fine-grained granitic facies, occurring, in some cases, as pod-shaped bodies (up to 1 meter in diameter; Fig. 3i). Alternation between aplite and pegmatite textures is common in these dikes (Fig. 3j). The mineralogy of pegmatites is mostly composed by euhedral to subhedral large crystals (centimeter to decimeter-large) of quartz, feldspar and biotite (Fig. 3i) and by millimeter-sized accessory garnet. Aplite dikes have centimeter- to decimeter-wide dimensions and are characterized by a very fine-grained (<0.1 cm) moderately equigranular xenomorphic texture with abundant garnet crystals as accessory mineral (Fig. 3k). The major mineral components in the mineralogy of aplites are: alkali feldspar, represented by anhedral microperthitic microcline crystals, rarely poikilitic (hosting smaller plagioclase and quartz grains), with weak undulatory extinction and weakly to well-developed sodic blebs; subhedral tabular plagioclase crystals with frequent polysynthetic twinning (Fig. 3l), and; anhedral crystals of quartz with moderate to strong undulatory extinction and irregular to slightly sutured boundaries (Fig. 3l). Biotite is also present as a minor component. It occurs as weakly to strongly chloritized anhedral to subhedral flakes showing strong pleochroism between pale yellow and brownish green, with a few pleochroic haloes. Garnet occurs as light brown euhedral to subhedral isolated octagon and/or dodecahedron-shaped crystals (<500 μm; Fig. 3k), in textural equilibrium with surrounding minerals. Other accessory minerals include Fe-Ti oxides, fluorite and sulfides.

3.2 Garnet Chemistry

The results of major element analysis of garnet grains from the MGI highly fractionated granitic rocks are listed in Supplementary File 2 and shown in Fig. 4. Overall, the abundance of garnet in the MGI highly fractionated granitic rocks increases from non-porphyritic garnet-bearing biotite granites (1 vol.%–2 vol.%) to aplite dikes (around 5 vol.%).

All garnet grains have high MnO (12.8 wt.%–28.1 wt.%) and FeO (8.1 wt.%–20.9 wt.%), but low MgO (<0.2 wt.%), TiO_2 (<0.7 wt.%) and low to moderate CaO (0.8 wt.%–12.4 wt.%) contents. Al_2O_3 is nearly constant in all the analyzed grains (19.7 wt.%–20.7 wt.%). They are mostly almandine–spessartine (63.7%–97.5% of the total molecular composition; Fig. 4).

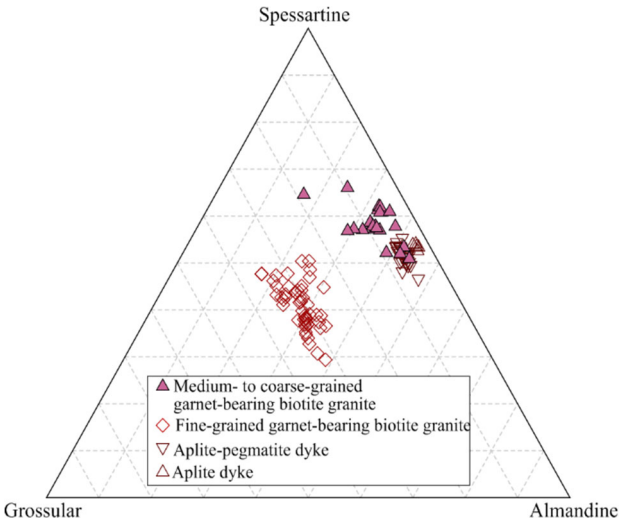

Figure 4. Ternary diagram showing the chemical composition of garnets from MGI highly fractionated granitic rocks in terms of the almandine, spessartine and grossular molecules.

However, garnet grains from a fine-grained garnet-bearing biotite granite depict a considerably higher grossular component (24.4%–34.5%; sample C71, see Fig. 4 and Supplementary File 2).

Electron microprobe data show that, while some crystals have relatively constant compositions, others have weak to moderate compositional zoning (Supplementary File 2). Among the latter, most grains are characterized by Mn-rich and Fe-poor cores and Mn-poor and Fe-rich rims. More rarely grains display oscillatory zoning patterns with variable MnO, FeO and CaO contents from rim to rim.

3.3 Whole-Rock Elemental Geochemistry

The whole-rock elemental data are listed in Supplementary File 3 (for details on the location of the analyzed samples see Supplementary File 4). According to their normative composition, the MGI highly fractionated granitic rocks vary between syenogranite to alkali feldspar granite (Fig. 5a). They have high SiO_2=73.47 wt.%–76.92 wt.%, moderate Al_2O_3 (12.17 wt.%–13.12 wt.%) and are relatively high in total alkalis, with K_2O=3.92 wt.%–5.01 wt.%, Na_2O=3.22 wt.%–4.26 wt.% and K_2O+Na_2O=7.65 wt.%–8.96 wt.%, plotting into the calc-alkaline series (Fig. 5b). Their A/CNK values range from 0.97 to 1.13, most of the samples being weakly peraluminous (Fig. 5c). They also have low contents of FeO^T (1.08–2.55; total Fe expressed as divalent), MgO (0.02 wt.%–0.08 wt.%), CaO (0.32 wt.%–0.99 wt.%), P_2O_5 (<0.07 wt.%), and TiO_2 (0.01 wt.%–0.08 wt.%), which tend to decrease with increasing SiO_2 contents. The $FeO^T/(FeO^T+MgO)$ ratios are relatively high, plotting into the ferroan granites field (Fig. 5d).

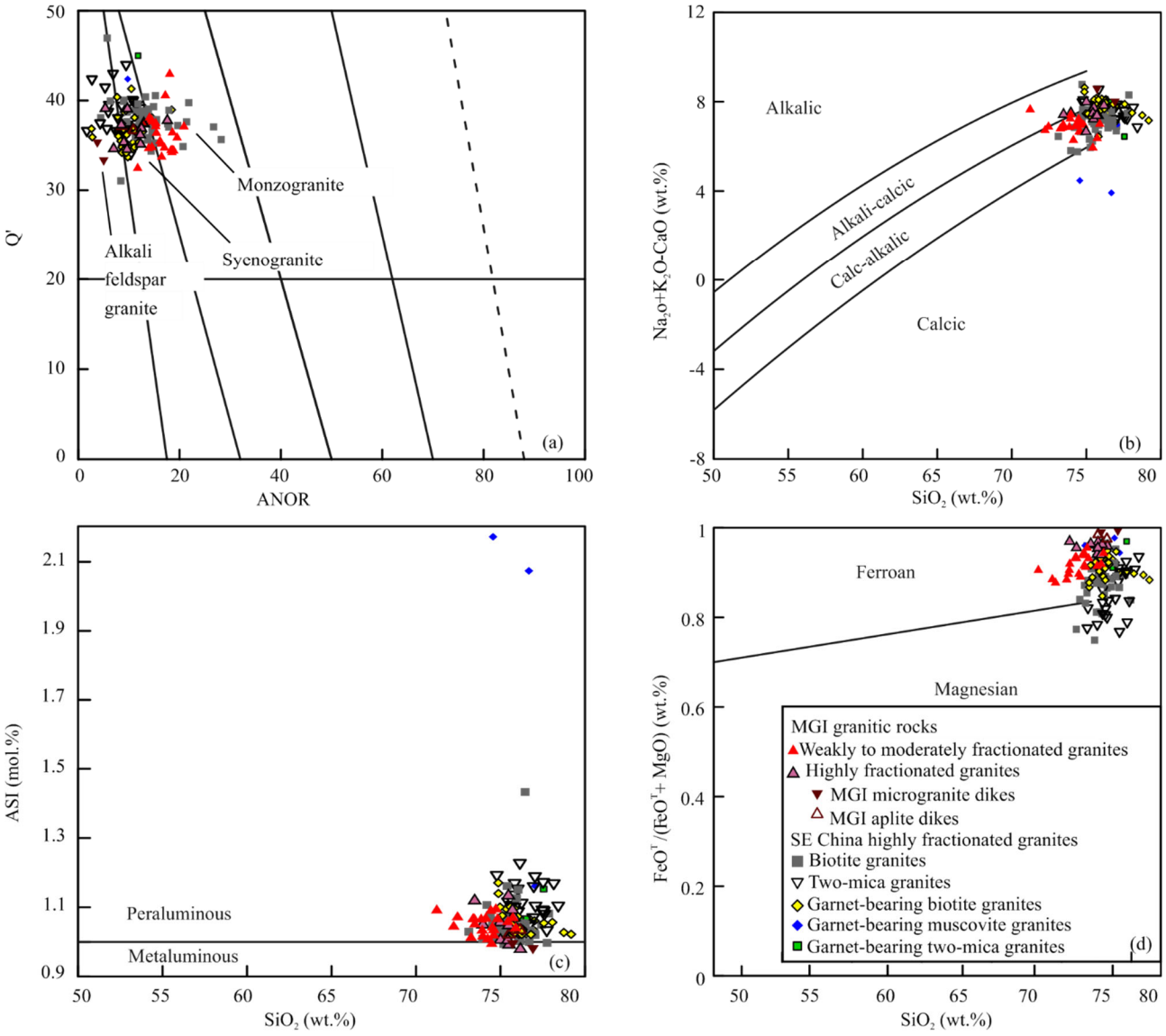

Figure 5. Classification diagrams for MGI and SE China Jurassic highly fractionated granitic rocks: (a) Q'-ANOR normative composition diagram (Streckeisen and Le Maitre, 1979), where Q'=Q/(Q+Or+Ab+An)×100; ANOR=An/(Or+An)×100; (b) Na_2O+K_2O-CaO vs. SiO_2 (Frost and Frost, 2008); (c) Aluminous Saturation Index [ASI or A/CNK defined as the molar ratio $Al_2O_3/(CaO+Na_2O+K_2O)$] vs. SiO_2; (d) $FeO^T/(FeO^T+MgO)$ vs. SiO_2 (Frost and Frost, 2008). SE China Jurassic highly fractionated granitic rocks with Zr/Hf≤25 (Jiang and Zhu, 2017; Zhang et al., 2017; Huang et al., 2015; Zhang et al., 2015; Huang et al., 2013; Guo et al., 2012; Li et al., 2007).

In the primitive mantle-normalized multi-element variation diagram (Fig. 6a), the MGI highly fractionated granitic rocks are characterized by enrichment in large ion lithophile elements (LILE; e.g., Rb, K, Pb, Th and U), with conspicuous negative Ba, Sr, P, Eu and Zr anomalies. While the MGI weakly to moderately fractionated granites tend to show depletion in high field strength elements (HFSE; e.g., Nb, Ta, and Ti), the MGI highly fractionated granites show enrichment in Nb, Ta, Pb, U, Y and heavy REE (HREE; Figs. 6a, 6b). The latter are also characterized by low Nb/Ta (2.71–5.65) and Zr/Hf (12.24–25.00) ratios similar to Jurassic highly fractionated granites outcropping in other regions of SE China (Li et al., 2007; Guo et al., 2012; Huang et al., 2013, 2015; Tao et al., 2013; Zhang et al., 2015, 2017; Jiang and Zhu, 2017).

The MGI highly fractionated granitic rocks also have moderate total REE contents (ΣREE=65.29 ppm–180.32 ppm) and show relatively flat (garnet-bearing biotite granites) to slightly positive slopes (garnet-bearing microgranite and aplite dikes) on chondrite-normalized REE patterns (Fig. 6b), with $(La/Yb)_N$=0.12–2.41, well-pronounced Eu anomalies (Eu/Eu*=0.02–0.19) and showing evidence for the tetrad effect ($TE_{1,3}$=1–1.12) as defined by Irber (1999). With the increase of SiO_2 content and decrease in Zr/Hf ratios, the HREE contents tend to increase and the Eu anomalies become more negative.

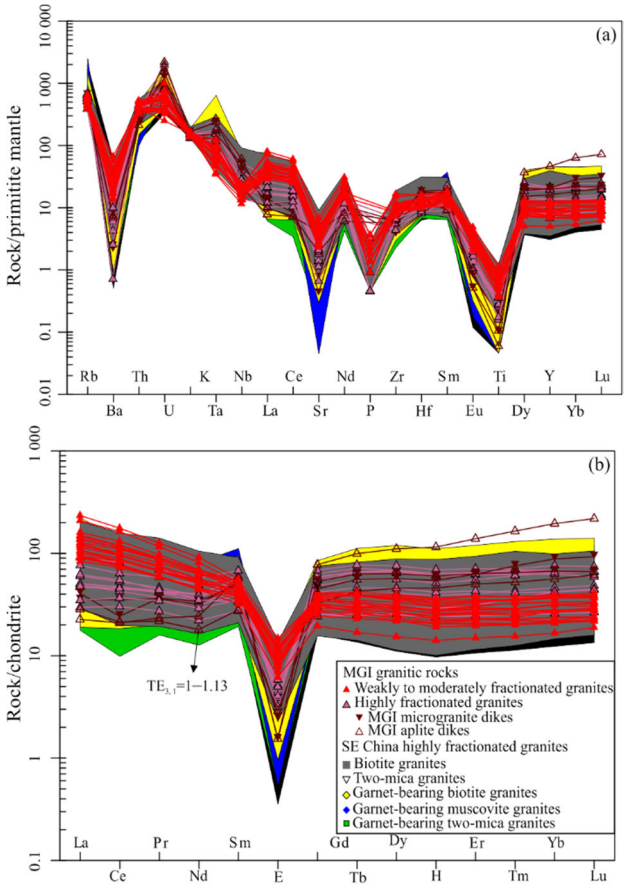

Figure 6. Primitive mantle (PM) normalized trace element spidergrams (PM values are from Sun and McDonough, 1989) (a) and; Chondrite normalized Rare Earth Elements (REE) patterns (chondrite values are from McDonough and Sun, 1995) (b) of MGI and SE China Jurassic highly fractionated granitic rocks.

Overall, the MGI highly fractionated granitic rocks have similar compositions to those of the SE China Jurassic highly fractionated. However, SE China Jurassic garnet-bearing biotite, muscovite and two-mica granites show more pronounced Eu and Sr anomalies (Figs. 6a, 6b), suggesting higher degrees of fractionation than those characterizing MGI highly fractionated granitic magmas. Some SE China Jurassic garnet-bearing muscovite granites can reach a strong peraluminous character (A/CNK up to ~2.2; Fig. 5c).

4 DISCUSSION

4.1 Differentiation Sequence of Highly Fractionated Granitic Rocks in Macao and SE China

The crystal fractionation processes underlying the evolution of Macao granites, in particular the influence of different major and accessory phases, have been addressed in detail by Quelhas et al. (2021). In this discussion, the aim is to unravel the differentiation sequence within the MGI highly fractionated rocks and frame it within the evolution of Jurassic highly fractionated granites in SE China. For this, we use Zr/Hf ratios, Rb, Sr, Ba and Eu concentration variation diagrams to assess the position of the different granitic facies in the fractionation series.

The Zr/Hf ratio has been regarded as a valuable differentiation index for granitic systems (Zaraisky et al., 2009; Irber, 1999) and was successfully applied to Macao granitic rocks in order to separate weakly to moderately fractionated facies (Zr/Hf ratios>25), and highly fractionated ones (Zr/Hf ratios≤25; Quelhas et al., 2021). As expected from their low Zr/Hf ratios, all the MGI highly fractionated granitic rocks plot into the strong differentiated granites field of the ternary diagram Ba-Sr-Rb (Fig. 7a). The trace element variation diagrams shown in Figs. 7b, 7c clearly show the influence of feldspar (s.l.) fractionation in the differentiation history of MGI and SE China granites. However, the variation in Ba contents points to a stronger influence of K-feldspar fractionation rather than plagioclase. Within the MGI granitic rocks, Sr and Ba is progressively depleted throughout the liquid line of descent producing the following lithological sequence: biotite granites, garnet-bearing biotite granites, microgranite dikes and lastly aplite dikes. Thus, the most fractionated magma in Macao is represented by the aplite-pegmatite dikes. However, coeval SE China Jurassic granites can reach even higher degrees of fractionation (Fig. 7). Indeed, while SE China biotite granites represent similar degrees of evolution as those of the MGI granites, SE China two-mica granites (Zr/Hf down to 12.24) can reach extremely low Ba (down to 3.53 ppm) and Sr (down to 0.94 ppm) contents and even more pronounced Eu anomalies (Eu/Eu* down to 0.03; Fig. 6b) than those characterizing the MGI highly fractionated granitic rocks (Eu/Eu* down to 0.13; Zr/Hf down to 8.88; Fig. 6b).

It has been shown by Quelhas et al. (2021) that fractionation of accessory phases such as allanite, monazite, xenotime, titanite, apatite and zircon, played an important role in the evolution of Macao granitic magmas. It is for example the case of the decrease in Th contents with increasing degree of evolution, *i.e.*, with the decrease of Zr/Hf ratios (Fig. 8a), which can be explained by fractionation of Th-bearing phases like xenotime and thorite. However, fractionation of these phases cannot explain the increase in Sm/Nd ratios (from 0.20 to 0.77) observed for

progressively more evolved MGI granitic rocks. Such increase in Sm/Nd, together with other peculiar chemical features of the MGI highly fractionated granitic rocks, is also observed for SE China Jurassic highly fractionated rocks (Sm/Nd=0.18–0.69), suggesting that Jurassic highly evolved magmas underwent evolution processes other than crystal fractionation.

4.2 Fluid/Melt Interaction in Highly Evolved Granitic Systems

As explained above, there are compositional characteristics of MGI granites, such as a significant enrichment in Nb, Ta, Pb, U, Y and HREE (Figs. 6a, 6b), that are hardly explained by crystal fractionation processes. A considerable enrichment in Rb is also observable for rocks with Zr/Hf<25 (Rb=214 ppm–1 578 ppm), leading to a significant decrease of K/Rb ratios in the melts (Fig. 8d). Such Rb enrichment in highly evolved granites is known to reflect autometasomatic processes caused by residual magmatic solutions (Gerstenberger, 1989).

It has long been known that highly evolved granitic magmas are characterized by physicochemical properties transitional between pure silicate melts and aqueous fluids (e.g., Monecke et al., 2007; Wu et al., 2004; Monecke et al., 2002; Jahn et al., 2001; Irber, 1999; Bau, 1996; Masuda et al., 1987). Chemical complexation with a wide variety of ligands, like non-bridging oxygen (e.g., F, B, P, etc.), changes significantly the melt structure and, consequently, the mineral/melt partition coefficients, promoting non-CHARAC (CHArge-and-RAdius-Controlled) behavior of HFSE (Bau, 1996).

MGI highly fractionated granitic rocks are characterized by non-chondritic ratios of Zr/Hf (12.24–25), K/Ba (498–9 560), K/Rb (101–158), La/Nb (0.15–2.18), La/Ta (0.69–11.32) and Nb/Ta (2.71–7.00; Fig. 8) strongly suggesting non-CHARAC behavior of trace elements, which is well evidenced in the Y/Ho vs. Zr/Hf diagram (Fig. 9a), where SE China Jurassic highly fractionated granitic rocks show a similar behavior.

Additionally, MGI and SE China Jurassic highly fractionated granitic rocks have REE patterns characterized by the presence of tetrad effects ($TE_{1,3}$ up to 1.13 and 1.22, respectively). Different processes have been proposed for the formation of the REE tetrad effect: (1) fractionation of accessory minerals (e.g., Pan, 1997; Pan and Breaks, 1997; Bau, 1996; McLennan, 1994; Zhao and Cooper, 1993; Yurimoto et al., 1990; Jolliff et al., 1989); (2) post-magmatic water-rock interactions (e.g., Takahashi et al., 2002; Masuda and Akagi, 1989), and (3) late-stage fluid/melt interactions (e.g., Tao et al., 2013; Wu et al., 2011; Monecke et al., 2007; Wu et al., 2004; Monecke et al., 2002; Zhao et al., 2002; Jahn et al., 2001; Irber, 1999; Bau, 1996), in particular with F-rich fluids (Badanina et al., 2006; Veksler et al., 2005).

Bau (1996) has shown that the tetrad effect cannot be adequately modelled with mineral/melt partition coefficients, which are smooth functions of ionic radii. Bau (1997) and Irber (1999) examined in the Nd-Sm decoupling and the tetrad effect in detail using Rayleigh model calculations and reported that mineral fractionation involving accessory phases failed to reproduce the tetrad effect-like REE pattern. This is also true for Macao, where Quelhas et al. (2021) showed that the observed increase of Sm/Nd ratios in MGI granitic rocks follows a distinct trend direction than that of monazite fractionation, an accessory phase that has been considered by some authors as capable of generating the REE tetrad effect (Duc-Tin and Keppler, 2015; Yurimoto et al., 1990).

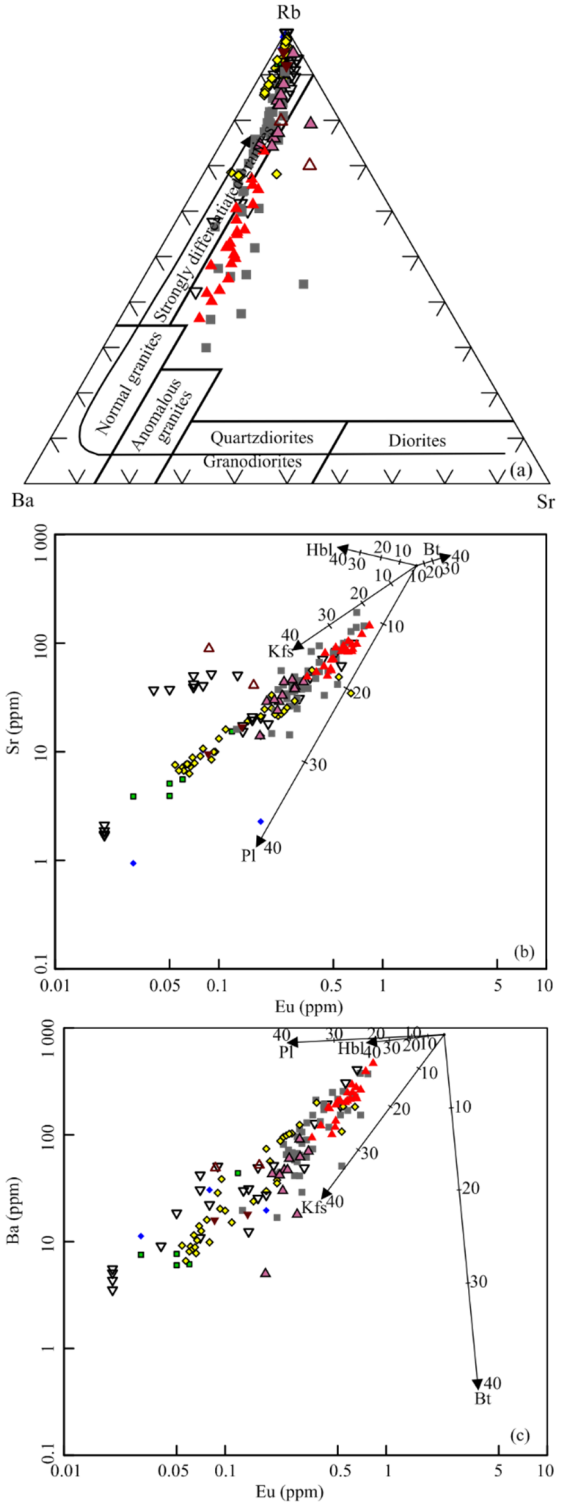

Figure 7. Trace element fractionation diagrams for MGI and SE China Jurassic highly fractionated granitic rocks: (a) Ba-Rb-Sr ternary diagram (El Bouseily and El Sokkary, 1975); (b) Sr vs. Eu; (c) Ba vs. Eu. Vectors represent the fractionation effect of different minerals calculated using partition coefficients from the literature (Bea et al., 1994; Bacon and Druitt, 1988; Nash and Crecraft, 1985). Kfs. Alkali feldspar; Pl. plagioclase; Bt. biotite; Hbl. hornblende. Symbols are as in Fig. 5.

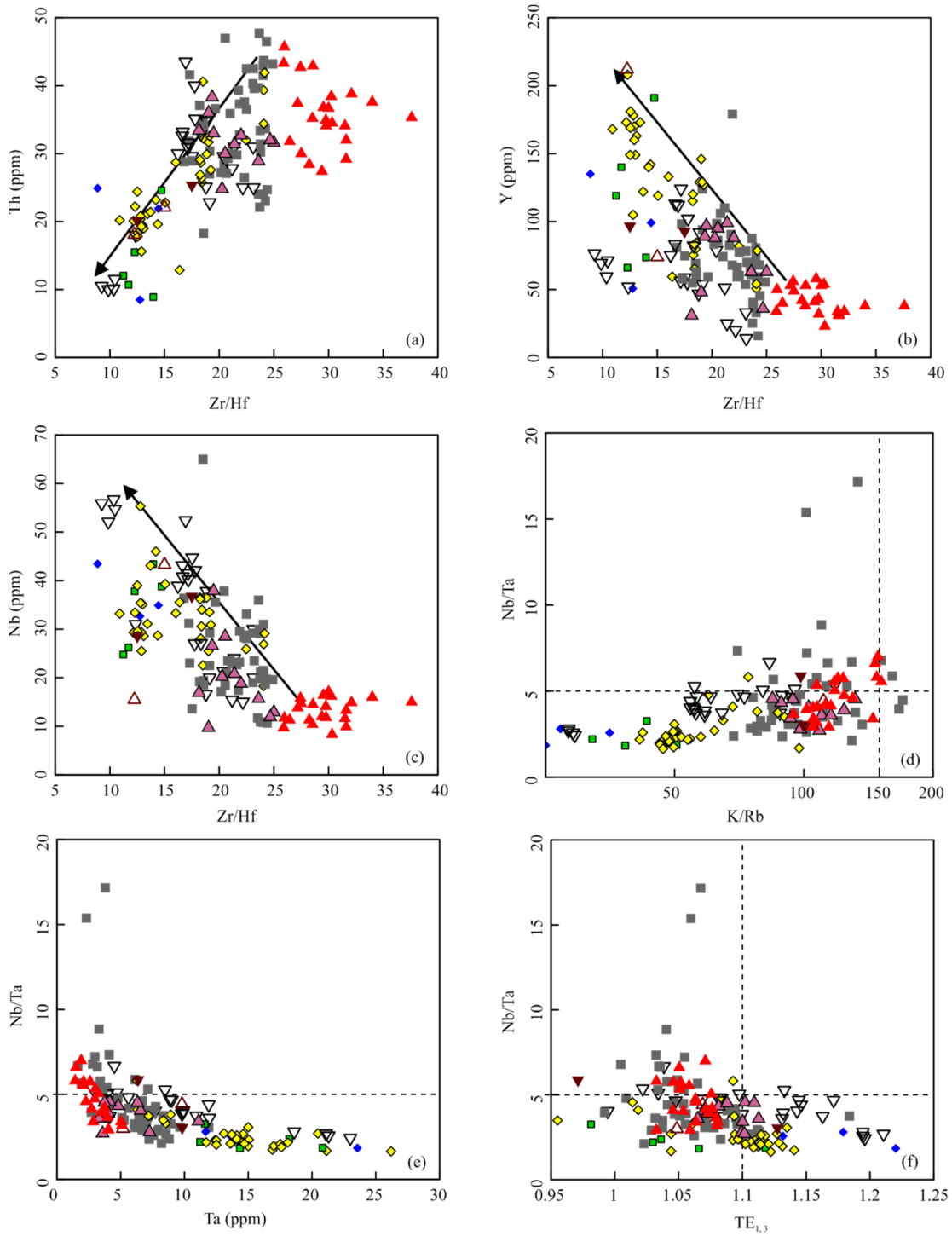

Figure 8. Trace element variation diagrams for MGI and SE China Jurassic highly fractionated granitic rocks: (a) Th vs. Zr/Hf; (b) Y vs. Zr/Hf; (c) Nb vs. Zr/Hf; (d) Nb/Ta vs. K/Rb; (e) Nb/Ta vs. Ta; (f) Nb/Ta vs. $TE_{3,1}$. The dashed lines represent the values of Nb/Ta (<5) and K/Rb (<150) which fingerprint the magmatic-hydrothermal transition in peraluminous granites (Ballouard et al., 2016); the dashed line for $TE_{3,1}$ represents the value above which the degree of the tetrad effect is considered significant (Irber, 1999). Symbols are as in Fig. 5.

Another argument against mineral fractionation as a common cause for the tetrad effect is based on accessory minerals that display tetrad effects that are similar to those of the host rocks (Wu et al., 2011; Zhao et al., 2002), indicating that the accessory mineral tetrad effect was inherited from a pre-existing melt tetrad effect rather than through a process of mineral fractionation.

Post-magmatic water-rock interaction is also unlikely since no REE tetrad effects have been observed in hydrothermally altered rocks that are not highly evolved (Jahn et al., 2001). Plus, analyses on some separated minerals show the same tetrad effects as their host rocks (Nardi et al., 2012; Wu et al., 2011; Zhao et al., 2002; Irber, 1999). This feature has thus a magmatic origin, inherited from the crystallization of magmas with the tetrad effect.

Fluid/melt interactions promote enrichment of volatiles and alkaline elements in the highly evolved granitic magmas, consequently lowering the solidus temperatures of the residual granitic system and leading to the formation of a co-existing magmatic-hydrothermal system (e.g., Peretyazhko and Savina 2010; Monecke et al. 2007; Irber 1999; Pan 1997; London et al. 1989). The volatile-enriched late magmatic fluids, having "W" type tetrad REE patterns, interact with the highly evolved melt and lead to the "M" type tetrad effect in the granites (Jahn et al., 2001; Irber, 1999), as observed for some of the more evolved granites, microgranites and aplites from Macao (Fig. 6b).

Fluorine (F) has been considered an important constituent of fluids inducing the REE tetrad effect on magmas with which they interact (Jiang H. et al., 2018; Xiang et al., 2017; Yang et al., 2017; Zhang et al., 2017; Bau and Dulski, 1995). Interestingly, some of the biotite grains from the MGI highly fractionated granites with the tetrad effect have relatively high F (up to 2.13 wt.%), similar to the F contents of muscovite from muscovite-bearing granites from SE China (F up to 2.25 wt.%; Zhang et al., 2017), and large crystals of purple fluorite have also been found in quartz veins cutting MGI granitic rocks (Quelhas et al., 2021). In addition, the more evolved coeval granites from surrounding areas of Macao show a progressive increase in Zr/Hf and Y/Ho ratios towards the Fluorite veins field (Fig. 9a). All these suggest that the late-stage fluid exsolved by the MGI and Jurassic SE China highly evolved granitic melts was rich in F.

Furthermore, the fluid/melt partition coefficients of Ta and Nb are low (D_{Nb} and D_{Ta} are 0–0.1 and 0.002–0.08, respectively; Zajacz et al., 2008; London et al., 1988), meaning that these elements are more compatible with the granitic magma than with the fluid and, thus, exsolution of the fluid from magma will increase the concentration of these elements in the magma (Linnen, 1998; Linnen and Keppler, 1997). The Nb and Ta contents of MGI granitic rocks remain nearly constant with decreasing Zr/Hf ratios, but suddenly increase for the MGI highly fractionated samples along with SE China granitic rocks with Zr/Hf≤25 and Nb/Ta<5 (Figs. 8c, 8e). Moreover, the fluid/melt partition coefficients mentioned above show more than one order of magnitude difference between Nb and Ta. This might explain the observed decrease in Nb/Ta ratios for MGI and SE China Jurassic highly fractionated rocks (Fig. 8d–f), which is accompanied by an increase in the degree of the REE tetrad effect (Fig. 8f). Therefore, we suggest that, along with the REE tetrad effect and the non-CHARAC behavior of trace elements, the main drive for Nb-Ta enrichment and fractionation in the MGI and SE China highly fractionated granitic magmas resulted from the exsolution and interaction of a F-rich fluid phase with the melt. Such process may also explain the increase in Y and HREE (Figs. 6, 8b) in the MGI highly fractionated granitic rocks, which favored the precipitation from the magma of mineral phases like fergusonite, gadolinite and columbite-tantalite. It is noteworthy that the highest enrichment in Y and HREE is observed in the aplites (Figs. 6b, 8b), where these mineral phases are more frequently found among MGI granitic rocks.

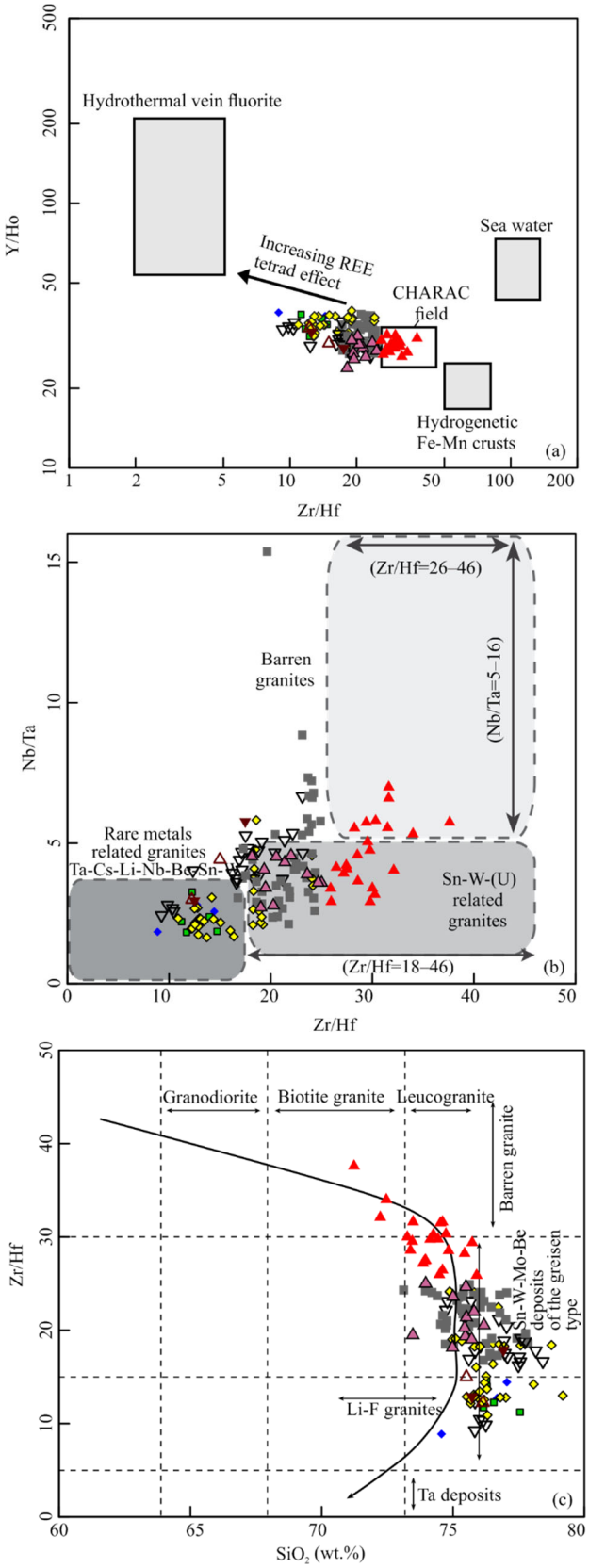

Figure 9. Trace element discriminant diagrams for MGI and SE China Jurassic highly fractionated granitic rocks: (a) Y/Ho vs. Zr/Hf (after Bau, 1996); (b) Nb/Ta vs. Zr/Hf (after Ballouard et al., 2016); (c) Zr/Hf vs. SiO_2 (after Zaraisky et al., 2009). Symbols are as in Fig. 5.

4.3 On the Genesis of Garnet from MGI Highly Fractionated Granitic Rocks

Overall, garnet from MGI highly fractionated granitic rocks occurs as euhedral to anhedral red-brownish grains, characterized by high FeO and MnO contents and often showing chemical zoning with spessartine-rich cores and almandine-rich rims or oscillatory zoning (Fig. 4; Supplementary File 2). Nevertheless, different garnet textures and chemistry point to the existence of two distinct types: small grossular-poor euhedral grains (Figs. 3k, 4) and much larger grossular-rich anhedral garnet grains with quartz inclusions (Figs. 3e, 4). The first type mostly occurs in aplitic facies, whereas the second type is mainly restricted to the fine- to medium-grained non-porphyritic garnet-bearing biotite granite (sample C71; see Fig. 4 and Supplementary File 2).

The origin of garnet in granitic rocks has been debated for many years, with different models being proposed: (1) refractory restite phase (René and Stelling, 2007); (2) peritectic entrainment phase from the zone of partial melting (Villaros et al., 2009; Stevens et al., 2007); (3) phenocrysts formed at high pressure (P≥7 kb) from mantle-derived magmas (Harangi et al., 2001; Green, 1992); (4) xenocrysts derived from partially assimilated metapelitic rocks (Lackey et al., 2012; Scallion et al., 2011; Erdmann et al., 2009; Fourcade et al., 2001); (5) precipitated phase from highly fractionated Mn-enriched peraluminous melts or from post-magmatic fluids through autometasomatic processes at low to moderate pressures (Speer and Becker, 1992; Whitworth, 1992; du Bray, 1988; Harrison, 1988; Kontak and Corey, 1988).

The occurrence of garnet in MGI granitic rocks is restricted to the highly fractionated facies, precluding the three first abovementioned origins. Despite peritectic garnet, texturally similar to the large skeletal garnet crystals of this study (Fig. 3e), has been reported in some S-type granites (e.g., Taylor and Stevens, 2010), this origin is unlikely in the case of MGI highly fractionated granites, as garnet is absent in the less evolved members of this group (*i.e.*, weakly to moderately fractionated facies). In addition, garnet formed at high-pressure usually has low MnO<3 wt.% (Harangi et al., 2001), in contrast with the high MnO contents of garnet from MGI (MnO=12.8 wt.%–28.1 wt.%). All these, together with the fact that garnet grains, in particular those from the first group (*i.e.*, grossular-poor garnet; Fig. 4) have no or few mineral inclusions and occur in textural equilibrium with other mineral phases, indicates crystallization from the host granitic magmas.

It has been recently proposed that the presence of garnet in Macao granites is suggestive of an origin through partial melting of sedimentary sources (Shellnut et al., 2020). Such interpretation is not consistent with the data and petrogenetic model published by Quelhas et al. (2021, 2020), in which Macao granites are interpreted as being derived from an infracrustal igneous source, for several reasons: (1) Sampling carried out by Shellnut et al. (2020) is concentrated in two specific areas of Macao, not being representative of the whole territory; (2) Shellnut et al. (2020) proposed an interpretation mainly based on the mineralogy and geochemistry of highly evolved granites from Macao (SiO_2=71.3 wt.%–79.1 wt.%; Rb/Sr=2–23), but did not take into account the characteristics of the coeval less evolved members of the magmatic sequence outcropping in Macao and surrounding areas (Quelhas et al., 2021, 2020; Huang et al., 2013; Zhang et al., 2015; Sewell et al., 1997). For instance, garnet only occurs in the highly fractionated granites of MGI, but not in more primitive co-genetic granites, clearly indicating a late-stage origin (Quelhas et al., 2021; this study); (3) Aluminous phases characteristic of S-type granites (e.g., muscovite and cordierite) are absent in Macao granites (Quelhas et al., 2021; this study), but hornblende, typical of I-type granites (Chappell and White, 1992), is present in coeval biotite granites and granodiorites in adjacent areas of Macao (e.g., Huang et al., 2013; Sewell et al., 1997); (4) Shellnut et al. (2020) has also suggested that the wide age range of inherited zircons present in weakly peraluminous granites (A/CNK<1.1) from Macao favors a sedimentary source. Yet, the percentage of inherited grains is much smaller compared with the magmatic zircon population (~95%; Quelhas et al., 2020), unlike what is commonly reported for highly peraluminous S-type granites (e.g., Miller et al., 2007, 2003); (4) The fact that two samples reported by Shellnut et al. (2020) have A/CNK slightly above 1.1, can be explained by higher fractionation degrees of more primitive I-type metaluminous to weakly-peraluminous magmas leading to an increase of the A/CNK of residual melts; (5) Shellnut et al. (2020) also used major [e.g., Molar $Al_2O_3/(MgO+FeO^T)$ vs. molar $CaO/(MgO+FeO^T)$] and trace (Rb/Ba vs. Rb/Sr) element ratios to argue for a sedimentary source. Due to high degrees of crystal fractionation, such elemental ratios in highly fractionated granites are not representative of the chemical composition of primary magmas and, consequently, not reliable to infer the source composition. Taking all these into account, the origin of garnet in Macao granites is not related with melting of sedimentary sources and the MGI highly fractionated granites (Zr/Hf<25) crystallized from highly evolved I-type granitic magmas.

The MGI highly fractionated rocks are slightly peraluminous (A/CNK up to 1.13) and have relatively high $MnO/(MnO+FeO^T)$ ratios (up to 0.86), conditions that favored the crystallization of Mn-rich garnet with percentages of spessartine molecule varying between 29.3% and 65.7%. Such features indicate that its crystallization occurred under low-pressure conditions (1–3 Kb; Green, 1977; Dahlquist et al., 2007; Speer and Becker, 1992; Clemens and Wall, 1988; Miller and Stoddard, 1982), in agreement with the intrusion of MGI granitic rocks in the upper crust. It has been proposed that assimilation of Mn-rich peraluminous materials in granitic magmas can promote crystallization of magmatic garnet (Scallion et al., 2011). Indeed, Quelhas et al. (2021) has reported the occurrence of Paleozoic metasedimentary enclaves enclosed within the MGI highly fractionated granites and also a relatively high percentage of inherited zircon with similar age in these granites (see also Quelhas et al., 2020). These evidences, together with the observed increase in initial $^{87}Sr/^{86}Sr$ ratios with degree of evolution observed for MGI, have led Quelhas et al. (2021) to propose that MGI granitic magmas assimilated metasedimentary materials during ascension and emplacement through assimilation-fractional crystallization (AFC) processes. Thus, assimilation of metasedimentary materials could have been a contributing factor to the formation of garnet in the MGI highly fractionated granitic magmas.

Zoning in garnet is strongly constrained by temperature variation during crystal growth (e.g., Li et al., 2017; Yardley, 1977). It has been suggested that magmatic garnets in granitic rocks crystallized above ~700 °C have "spessartine inverse bell-shaped profiles" (Mn-poor cores and Mn-rich rims) or are unzoned, whereas garnets exhibiting "spessartine bell-shaped profile" must have been formed in highly felsic magmas (SiO_2=73 wt.%–76 wt.%) crystallizing below ~700 °C (Dahlquist et al., 2007). The garnet crystals in MGI highly fractionated granitic rocks are either unzoned or characterized by a "spessartine bell-shaped profile" (Mn-rich cores and Mn-poor rims) suggesting their crystallization either above or below 700 ºC, respectively. This is endorsed by the range of zircon saturation temperatures (T_{Zr}=691.1–735.4 ºC; Supplementary File 3) calculated for the MGI highly fractionated granitic rocks. Although the presence of significant amounts of inherited zircon component can lead to an overestimation of magma temperatures (e.g., Miller et al., 2003), this is not the case for Macao granitic rocks where the dominant zircon population is of magmatic origin (Quelhas et al., 2020).

The second type of garnet has significantly higher CaO contents, which translates into a higher grossular component (24.4%–34.5%; Fig. 4). These garnet crystals occur with a distinct habit, characterized by large sizes (up to 5 mm; Fig. 3d) and skeletal shapes forming garnet-quartz intergrowths (Fig. 3e), suggesting late-stage replacement of the primary granite mineralogy by garnet through metasomatic processes (Kontak and Corey, 1988). Such process would require the local gain of Fe, Ca, Al and Mn provided by the interaction of magmatic fluids with previously crystallized mineral phases (*i.e.*, quartz, biotite, K-feldspar and plagioclase), though an extraneous component derived from the interaction of these fluids with assimilated metasedimentary enclaves or surrounding metasedimentary strata cannot be ruled out. In the latter case, it has been proposed that the circulating fluid breaks down and dissolves plagioclase from the surrounding lithologies, becomes more aluminous, acidic and Ca-bearing, eventually re-entering and introducing foreign elements (e.g., Ca, Fe and Mg) into the highly evolved granitic body (Martin and De Vito, 2014). This could also account for the oscillatory zoning of some garnet crystals (e.g., sample c71_b5_grt; Supplementary File 2), as this kind of compositional zoning often reflects oscillatory changes in the fluid composition that may be internally and/or externally controlled (e.g., Ranjbar et al., 2016; Ríos Reyes et al., 2009). Oscillatory zoning requires that the fluid flow is episodic and, possibly, accompanied by periods of reduced growth rates between individual pulses of channelized hydrothermal fluid flow (Dziggel et al., 2009).

The transition from magmatic to metasomatic garnets in MGI highly fractionated granites thus reinforces the role of fluids as a controlling factor in the chemistry and mineralogy of late-stage highly evolved granitic rocks. We propose that increasing CaO contents of late-stage crystallized garnets in granitic rocks may reflect a progressively stronger influence of fluids in their composition.

4.4 A Brief Comment on the Mineralization Potential of Macao Granitic Rocks

The Jurassic magmatic activity, particularly at 165–150 Ma, produced widespread highly differentiated granitic magmas in the Cathaysia Block, some of them clearly more evolved than the Macao counterparts.

The Zr/Hf and Nb/Ta ratios have been considered good indicators of potential mineralization in granitic rocks (Ballouard et al., 2016; Zaraisky et al., 2009). The MGI weakly to moderately fractionated granites straddle the limit between "barren granites" and "mineralized granites" fields (Fig. 9b and c). The MGI highly fractionated granitic rocks, on the other hand, have trace element features similar to Sn-W-(U)-Mo-Be related granites (Figs. 9b, 9c), suggesting that this facies has the potential for mineralization and most likely corresponds to the first stage of tungsten (W) mineralization in SE China during the Jurassic (e.g., Mao et al., 2013; Wang et al., 2011). Moreover, spessartine-rich garnet tends to be less abundant in biotite granites (such as those represented by MGI highly fractionated granites) than it is in the two-mica granites and muscovite granites, which are the main host rocks of tungsten deposits in SE China (Zhang et al., 2017; Guo et al., 2012). In MGI highly fractionated granites, however, no W-bearing phases have been observed. Thus, higher degrees of fractional crystallization coupled with fluid/melt interactions progressively enriched the granitic magmas in W (and also Sn, U, Nb-Ta and REE; Jiang et al., 2017; this study), which has been confirmed by increasing whole-rock W concentrations from the garnet-free biotite granites to garnet-bearing muscovite granites in the Nanling Range, SE China (Zhang et al., 2017). This might explain why the large-scale polymetallic mineralization is closely associated with the muscovite-bearing granites rather than biotite granites in Macao and SE China.

We thus propose that the stage of evolution represented by the MGI highly fractionated granitic rocks corresponds to the onset of fluid/melt interaction in a highly evolved granitic system, which led to enhanced hydrothermal activity and consequent widespread mineralization in the more evolved lithotypes (e.g., two-mica granites and garnet muscovite granites) of the Jurassic differentiation sequence in SE China (Figs. 9b, 9c; e.g., Jiang and Zhu, 2017; Zhang et al., 2017; Huang et al., 2015; Zhang et al., 2015; Huang et al., 2013; Guo et al., 2012; Li et al., 2007). Although other authors have proposed different Zr/Hf threshold values for the beginning of mineralization in a granitic system (Zr/Hf=46 and Zr/Hf=30; Zaraisky et al., 2009 and Ballouard et al., 2016, respectively), our data suggest that the values of Zr/Hf≤25, characterizing the non-CHARAC behavior of these elements (Bau, 1996), along with those of Nb/Ta<5 (Ballouard et al., 2016; this study), mark a significant increase in mineralization potential of granitic systems due to fluid/melt interactions at late-stage magma evolution.

5 CONCLUSIONS

(1) The differentiation sequence in Macao is as follows: biotite granites, garnet-bearing biotite granites, microgranite dikes and lastly aplite (and pegmatite) dikes. Our study suggests that the ~160 Ma granitic magmas in SE China reached even higher degrees of evolution, forming two-mica granites and garnet-bearing biotite and muscovite granites in surrounding areas of Macao.

(2) High degrees of fractionation coupled with fluid/melt interactions, involving magmatic F-rich fluids, was the

cause for the observed non-CHARAC behavior of trace elements, leading, for example, to non-chondritic Zr/Hf ratios, REE tetrad effect and Nb-Ta enrichment and fractionation in the MGI and SE China highly fractionated granitic magmas.

(3) Two populations of garnet, with distinct textural and chemical features, were identified in MGI highly fractionated granitic rocks: small grossular-poor euhedral grains and large grossular-rich skeletal garnet grains with quartz inclusions. The first group was formed through precipitation from highly evolved Mn-rich slightly peraluminous melts under low-pressure and relatively low temperature (~700 ºC) conditions. Assimilation of upper crust metasedimentary materials may have contributed as a source of Mn and Al to the formation of garnet. The second group has a metasomatic origin related to the interaction of magmatic fluids with previously crystallized mineral phases (*i.e*., quartz, biotite, K-feldspar and plagioclase) and, possibly, with assimilated metasedimentary enclaves or surrounding metasedimentary strata. We propose that increasing CaO contents of late-stage crystallized garnets in granitic rocks may reflect a progressively stronger influence of fluids in their composition.

(4) The stage of evolution represented by the MGI highly fractionated granitic rocks corresponds to the onset of fluid/melt interaction in a highly evolved granitic system, which led to enhanced hydrothermal activity and consequent W-(Mo)-Sn-Nb-Ta polymetallic mineralization in the more evolved lithotypes (e.g., two-mica granites and garnet muscovite granites) of the Jurassic magmatic differentiation sequence in SE China. Zr/Hf≤25 and Nb/Ta<5 may be important thresholds to identify granite-related mineral deposits, particularly in the SE China region.

ACKNOWLEDGEMENTS

This research was supported by the Macao Science and Technology Development Fund (No. FDCT 043/2014/A1). We acknowledge the financial FCT support through project UIDB/50019/2020–IDL. We are very grateful to Varon Lou (Lou U. Tat) and Ricardo Borges for their important help during the field and lab work and to Pedro Rodrigues for skilled assistance during electron microprobe analyses. We thank the two anonymous reviewers for their useful comments that greatly improved the manuscript. The final publication is available at Springer via https://doi.org/10.1007/s12583-020-1389-4.

Electronic Supplementary Materials: Supplementary materials (Supplementary Files 1, 2, 3, 4) are available in the online version of this article at https://doi.org/10.1007/s12583-020-1389-4.

REFERENCES CITED

Antunes, I. M. H. R., Neiva, A. M. R., Ramos, J. M. F., et al., 2013. Petrogenetic Links between Lepidolite-Subtype Aplite-Pegmatite, Aplite Veins and Associated Granites at Segura (Central Portugal). *Geochemistry*, 73(3): 323–341. https://doi.org/10.1016/j.chemer.2012.12.003

Bacon, C. R., Druitt, T. H, 1988. Compositional Evolution of the Zoned Calcalkaline Magma Chamber of Mount Mazama, Crater Lake, Oregon. *Contributions to Mineralogy and Petrology*, 98(2): 224–256. https://doi.org/10.1007/bf00402114

Badanina, E. V., Trumbull, R. B., Dulski, P., et al., 2006. The Behavior of rare-Earth and Lithophile Trace Elements in rare-Metal Granites: a Study of Fluorite, Melt Inclusions and Host Rocks from the Khangilay Complex, Transbaikalia, Russia. *The Canadian Mineralogist*, 44(3): 667–692. https://doi.org/10.2113/gscanmin.44.3.667

Ballouard, C., Poujol, M., Boulvais, P., et al., 2016. Nb-Ta Fractionation in Peraluminous Granites: A Marker of the Magmatic-Hydrothermal Transition. *Geology*, 44(3): 231–234. https://doi.org/10.1130/g37475.1

Bau, M, 1997. The Lanthanide Tetrad Effect in Highly Evolved Felsic Igneous Rocks—A Reply to the Comment by Y. Pan. *Contributions to Mineralogy and Petrology*, 128(4): 409–412. https://doi.org/10.1007/s004100050318

Bau, M., Dulski, P, 1995. Comparative Study of Yttrium and Rare-Earth Element Behaviours in Fluorine-Rich Hydrothermal Fluids. *Contributions to Mineralogy and Petrology*, 119(2/3): 213–223. https://doi.org/10.1007/BF00307282

Bea, F., Pereira, M. D., Stroh, A, 1994. Mineral/Leucosome Trace-Element Partitioning in a Peraluminous Migmatite (a Laser Ablation-ICP-MS Study). *Chemical Geology*, 117(1/2/3/4): 291–312. https://doi.org/10.1016/0009-2541(94)90133-3

Bray, E. A, 1988. Garnet Compositions and Their Use as Indicators of Peraluminous Granitoid Petrogenesis—Southeastern Arabian Shield. *Contributions to Mineralogy and Petrology*, 100(2): 205–212. https://doi.org/10.1007/BF00373586

Cao, J. Y., Yang, X. Y., Du, J. G., et al., 2018. Formation and Geodynamic Implication of the Early Yanshanian Granites Associated with W-Sn Mineralization in the Nanling Range, South China: An Overview. *International Geology Review*, 60(11/12/13/14): 1744–1771. https://doi.org/10.1080/00206814.2018.1466370

Carrington da Costa, J., Lemos, M.S., 1964. Fisiografia e Geologia da Província de Macau. Centro Municipal de Informação de Turismo

Chappell, B. W., White, A. J. R, 1992. I- and S-Type Granites in the Lachlan Fold Belt. *Earth and Environmental Science Transactions of the Royal Society of Edinburgh*, 83(1/2): 1–26. https://doi.org/10.1017/s0263593300007720

Charvet, J, 2013. The Neoproterozoic–Early Paleozoic Tectonic Evolution of the South China Block: An Overview. *Journal of Asian Earth Sciences*, 74: 198–209. https://doi.org/10.1016/j.jseaes.2013.02.015

Chen, G.-N., Grapes, R., 2007. Granite Genesis: In Situ Melting and Crustal Evolution. Elsevier, Netherlands. 276

Clemens, J. D., Wall, V. J, 1988. Controls on the Mineralogy of S-Type Volcanic and Plutonic Rocks. *Lithos*, 21(1): 53–66. https://doi.org/10.1016/0024-4937(88)90005-9

Costa, J.C.D.A., 1944. Geologia da Província de Macau. Boletim da Sociedade Geológica de Portugal, 3: 181–222

Dahlquist, J. A., Galindo, C., Pankhurst, R. J., et al., 2007. Magmatic Evolution of the Peñón Rosado Granite: Petrogenesis of Garnet-Bearing Granitoids. *Lithos*, 95(3/4): 177–207. https://doi.org/10.1016/j.lithos.2006.07.010

Dill, H. G, 2015. Pegmatites and Aplites: Their Genetic and Applied Ore Geology. *Ore Geology Reviews*, 69: 417–561. https://doi.org/10.1016/j.oregeorev.2015.02.022

Duc-Tin, Q., Keppler, H, 2015. Monazite and Xenotime Solubility in Granitic Melts and the Origin of the Lanthanide Tetrad Effect. *Contributions to Mineralogy and Petrology*, 169(1): 1–26. https://doi.org/10.1007/s00410-014-1100-9

Dziggel, A., Wulff, K., Kolb, J., et al., 2009. Significance of Oscillatory and Bell-Shaped Growth Zoning in Hydrothermal Garnet: Evidence from the Navachab Gold Deposit, Namibia. *Chemical Geology*, 262(3/4): 262–

276. https://doi.org/10.1016/j.chemgeo.2009.01.027

El Bouseily, A. M., El Sokkary, A. A, 1975. The Relation between Rb, Ba and Sr in Granitic Rocks. *Chemical Geology*, 16(3): 207–219. https://doi.org/10.1016/0009-2541(75)90029-7

Erdmann, S., Jamieson, R. A., MacDonald, M. A, 2009. Evaluating the Origin of Garnet, Cordierite, and Biotite in Granitic Rocks: a Case Study from the South Mountain Batholith, Nova Scotia. *Journal of Petrology*, 50(8): 1477–1503. https://doi.org/10.1093/petrology/egp038

Fourcade, S., Capdevila, R., Ouabadi, A., et al., 2001. The Origin and Geodynamic Significance of the Alpine Cordierite-Bearing Granitoids of Northern Algeria. A Combined Petrological, Mineralogical, Geochemical and Isotopic (O, H, Sr, Nd) Study. *Lithos*, 57(2/3): 187–216. https://doi.org/10.1016/s0024-4937(01)00034-2

Frost, B. R., Frost, C. D, 2008. A Geochemical Classification for Feldspathic Igneous Rocks. *Journal of Petrology*, 49(11): 1955–1969. https://doi.org/10.1093/petrology/egn054

Gerstenberger, H, 1989. Autometasomatic Rb Enrichments in Highly Evolved Granites Causing Lowered Rb Sr Isochron Intercepts. *Earth and Planetary Science Letters*, 93(1): 65–75. https://doi.org/10.1016/0012-821x(89)90184-2

Green, T. H, 1977. Garnet in Silicic Liquids and Its Possible Use as a P-T Indicator. *Contributions to Mineralogy and Petrology*, 65(1): 59–67. https://doi.org/10.1007/BF00373571

Green, T.H., 1992. Experimental Phase Equilibrium Studies of Garnet-Bearing I-Type Volcanics and High-Level Intrusives from Northland, New Zealand. Geological Society of America Special Papers. *Geological Society of America*, 272: 429–438. https://doi.org/10.1130/spe272-p429

Guo, C. L., Chen, Y. C., Zeng, Z. L., et al., 2012. Petrogenesis of the Xihuashan Granites in Southeastern China: Constraints from Geochemistry and In-Situ Analyses of Zircon U-Pb-Hf-O Isotopes. *Lithos*, 148: 209–227. https://doi.org/10.1016/j.lithos.2012.06.014

Harangi, S., Downes, H., Kósa, L., et al., 2001. Almandine Garnet in Calc-Alkaline Volcanic Rocks of the Northern Pannonian Basin (Eastern-Central Europe): Geochemistry, Petrogenesis and Geodynamic Implications. *Journal of Petrology*, 42(10): 1813–1843. https://doi.org/10.1093/petrology/42.10.1813

Harrison, T. N, 1988. Magmatic Garnets in the Cairngorm Granite, Scotland. *Mineralogical Magazine*, 52(368): 659–667. https://doi.org/10.1180/minmag.1988.052.368.10

Huang, H. Q., Li, X. H., Li, Z. X., et al., 2013. Intraplate Crustal Remelting as the Genesis of Jurassic High-K Granites in the Coastal Region of the Guangdong Province, SE China. *Journal of Asian Earth Sciences*, 74: 280–302. https://doi.org/10.1016/j.jseaes.2012.09.009

Huang, H. Q., Li, X. H., Li, Z. X., et al., 2015. Formation of the Jurassic South China Large Granitic Province: Insights from the Genesis of the Jiufeng Pluton. *Chemical Geology*, 401: 43–58. https://doi.org/10.1016/j.chemgeo.2015.02.019

Irber, W, 1999. The Lanthanide Tetrad Effect and Its Correlation with K/Rb, Eu/Eu, Sr/Eu, Y/Ho, and Zr/Hf of Evolving Peraluminous Granite Suites. *Geochimica et Cosmochimica Acta*, 63(3/4): 489–508. https://doi.org/10.1016/s0016-7037(99)00027-7

Jahn, B. M., Wu, F. Y., Capdevila, R., et al., 2001. Highly Evolved Juvenile Granites with Tetrad REE Patterns: The Woduhe and Baerzhe Granites from the Great Xing'an Mountains in NE China. *Lithos*, 59(4): 171–198. https://doi.org/10.1016/s0024-4937(01)00066-4

Jahns, R.H., Tuttle, O.F., 1963. Layered Pegmatite-Aplite Intrusives. Mineralogical Society of America Special Paper, 1: 78–92

Jiang, H., Jiang, S. Y., Li, W. Q., et al., 2018. Highly Fractionated Jurassic I-Type Granites and Related Tungsten Mineralization in the Shirenzhang Deposit, Northern Guangdong, South China: Evidence from Cassiterite and Zircon U-Pb Ages, Geochemistry and Sr-Nd-Pb-Hf Isotopes. *Lithos*, 312/313: 186–203. https://doi.org/10.1016/j.lithos.2018.04.030

Jiang, W. C., Li, H., Wu, J. H., et al., 2018. A Newly Found Biotite Syenogranite in the Huangshaping Polymetallic Deposit, South China: Insights into Cu Mineralization. *Journal of Earth Science*, 29(3): 537–555. https://doi.org/10.1007/s12583-017-0974-7

Jiang, Y. H., Jiang, S. Y., Dai, B. Z., et al., 2009. Middle to Late Jurassic Felsic and Mafic Magmatism in Southern Hunan Province, Southeast China: Implications for a Continental Arc to Rifting. *Lithos*, 107(3/4): 185–204. https://doi.org/10.1016/j.lithos.2008.10.006

Jiang, Y. H., Zhu, S. Q, 2017. Petrogenesis of the Late Jurassic Peraluminous Biotite Granites and Muscovite-Bearing Granites in SE China: Geochronological, Elemental and Sr-Nd-O-Hf Isotopic Constraints. *Contributions to Mineralogy and Petrology*, 172(11/12): 1–27. https://doi.org/10.1007/s00410-017-1422-5

Jolliff, B. L., Papike, J. J., Shearer, C. K., et al., 1989. Inter- and Intra-Crystal REE Variations in Apatite from the Bob Ingersoll Pegmatite, Black Hills, South Dakota. *Geochimica et Cosmochimica Acta*, 53(2): 429–441. https://doi.org/10.1016/0016-7037(89)90394-3

Kontak, D.J., Corey, M., 1988. Metasomatic origin of spessartine-rich garnet in the South Mountain Batholith, Nova Scotia. Canadian Mineralogist, 26, 315-334.

Lackey, J. S., Romero, G. A., Bouvier, A. S., et al., 2012. Dynamic Growth of Garnet in Granitic Magmas. *Geology*, 40(2): 171–174. https://doi.org/10.1130/g32349.1

Li, B. W., Ge, J. H., Zhang, B. H, 2018. Diffusion in Garnet: a Review. *Acta Geochimica*, 37(1): 19–31. https://doi.org/10.1007/s11631-017-0187-x

Li, X. H., Li, Z. X., Li, W. X., et al., 2007. U–Pb Zircon, Geochemical and Sr–Nd–Hf Isotopic Constraints on Age and Origin of Jurassic I- and A-Type Granites from Central Guangdong, SE China: a Major Igneous Event in Response to Foundering of a Subducted Flat-Slab? *Lithos*, 96(1/2): 186–204. https://doi.org/10.1016/j.lithos.2006.09.018

Li, Z. X., Li, X. H., 2007. Formation of the 1300-Km-Wide Intracontinental Orogen and Postorogenic Magmatic Province in Mesozoic South China: a Flat-Slab Subduction Model. *Geology*, 35(2): 179. https://doi.org/10.1130/g23193a.1

Li, Z. X., Li, X. H., Zhou, H. W., et al., 2002. Grenvillian Continental Collision in South China: New SHRIMP U-Pb Zircon Results and Implications for the Configuration of Rodinia. *Geology*, 30(2): 163. https://doi.org/10.1130/0091-7613(2002)0300163: gccisc>2.0.co;2

Linnen, R. L, 1998. The Solubility of Nb-Ta-Zr-Hf-W in Granitic Melts with Li and Li+F; Constraints for Mineralization in Rare Metal Granites and Pegmatites. *Economic Geology*, 93(7): 1013–1025. https://doi.org/10.2113/gsecongeo.93.7.1013

Linnen, R. L., Keppler, H, 1997. Columbite Solubility in Granitic Melts: Consequences for the Enrichment and Fractionation of Nb and Ta in the Earth's Crust. *Contributions to Mineralogy and Petrology*, 128(2/3): 213–227. https://doi.org/10.1007/s004100050304

London, D, 1992. The Application of Experimental Petrology to the Genesis and Crystallization of Granitic Pegmatites. *Canadian Mineralogist*, 30(3): 499–540.

London, D, 2014. A Petrologic Assessment of Internal Zonation in Granitic Pegmatites. *Lithos*, 184/185/186/187: 74–104. https://doi.org/10.1016/j.lithos.2013.10.025

London, D., 2008. Pegmatites. Canadian Mineralogist, Special Publication, 10: 347

London, D., Hervig, R. L., Morgan, G. B, 1988. Melt-Vapor Solubilities and Elemental Partitioning in Peraluminous Granite-Pegmatite Systems: Experimental Results with Macusani Glass at 200 MPa. *Contributions to Mineralogy and Petrology*, 99(3): 360–373. https://doi.org/10.1007/BF00375368

London, D., Kontak, D. J, 2012. Granitic Pegmatites: Scientific Wonders and Economic Bonanzas. *Elements*, 8(4): 257–261. https://doi.org/10.2113/gselements.8.4.257

London, D., Morgan, G. B., Hervig, R. L, 1989. Vapor-Undersaturated Experiments with Macusani glass+H_2O at 200 MPa, and the Internal Differentiation of Granitic Pegmatites. *Contributions to Mineralogy and Petrology*, 102(1): 1–17. https://doi.org/10.1007/BF01160186

London, D., Morgan, G. B., Paul, K. A., et al., 2012. Internal Evolution of Miarolitic Granitic Pegmatites at the Little Three Mine, Ramona, California, USA. *The Canadian Mineralogist*, 50(4): 1025–1054. https://doi.org/10.3749/canmin.50.4.1025

Lowenstern, J. B, 1994. Dissolved Volatile Concentrations in an Ore-Forming Magma. *Geology*, 22(10): 893. https://doi.org/10.1130/0091-7613(1994)0220893: dvciao>2.3.co;2

Mao, J. W., Cheng, Y. B., Chen, M. H., et al., 2013. Major Types and Time-Space Distribution of Mesozoic Ore Deposits in South China and Their Geodynamic Settings. *Mineralium Deposita*, 48(3): 267–294. https://doi.org/10.1007/s00126-012-0446-z

Martin, R. F., de Vito, C, 2014. The Late-Stage Miniflood of ca in Granitic Pegmatites: An Open-System Acid-Reflux Model Involving Plagioclase in the Exocontact. *The Canadian Mineralogist*, 52(2): 165–181. https://doi.org/10.3749/canmin.52.2.165

Masuda, A., Akagi, T, 1989. Lanthanide Tetrad Effect Observ Ed in Leucogranites from China. *Geochemical Journal*, 23(5): 245–253. https://doi.org/10.2343/geochemj.23.245

Masuda, A., Kawakami, O., Dohmoto, Y., et al., 1987. Lanthanide Tetrad Effects in Nature: Two Mutually Opposite Types, W and M. *Geochemical Journal*, 21(3): 119–124. https://doi.org/10.2343/geochemj.21.119

McDonough, W. F., Sun, S. S, 1995. The Composition of the Earth. *Chemical Geology*, 120(3/4): 223–253. https://doi.org/10.1016/0009-2541(94)00140-4

McLennan, S. M, 1994. Rare Earth Element Geochemistry and the "Tetrad" Effect. *Geochimica et Cosmochimica Acta*, 58(9): 2025–2033. https://doi.org/10.1016/0016-7037(94)90282-8

Miller, C. F., McDowell, S. M., Mapes, R. W, 2003. Hot and Cold Granites? Implications of Zircon Saturation Temperatures and Preservation of Inheritance. *Geology*, 31(6): 529–532. https://doi.org/10.1130/0091-7613(2003)0310529: hacgio>2.0.co;2

Miller, C. F., Stoddard, E. F., 1982. The Role of Manganese in the Paragenesis of Magmatic Garnet: An Example from the Old Woman-Piute Range, California, *Journal of Geology*, 90: 341–343

Miller, J. S., Matzel, J. E. P., Miller, C. F., et al., 2007. Zircon Growth and Recycling during the Assembly of Large, Composite Arc Plutons. *Journal of Volcanology and Geothermal Research*, 167(1/2/3/4): 282–299. https://doi.org/10.1016/j.jvolgeores.2007.04.019

Monecke, T., Dulski, P., Kempe, U, 2007. Origin of Convex Tetrads in Rare Earth Element Patterns of Hydrothermally Altered Siliceous Igneous Rocks from the Zinnwald Sn-W Deposit, Germany. *Geochimica et Cosmochimica Acta*, 71(2): 335–353. https://doi.org/10.1016/j.gca.2006.09.010

Monecke, T., Kempe, U., Monecke, J., et al., 2002. Tetrad Effect in Rare Earth Element Distribution Patterns: A Method of Quantification with Application to Rock and Mineral Samples from Granite-Related Rare Metal Deposits. *Geochimica et Cosmochimica Acta*, 66(7): 1185–1196. https://doi.org/10.1016/s0016-7037(01)00849-3

Nabelek, P. I., Whittington, A. G., Sirbescu, M. L. C, 2010. The Role of H_2O in Rapid Emplacement and Crystallization of Granite Pegmatites: Resolving the Paradox of Large Crystals in Highly Undercooled Melts. *Contributions to Mineralogy and Petrology*, 160(3): 313–325. https://doi.org/10.1007/s00410-009-0479-1

Nardi, L. V. S., Formoso, M. L. L., Jarvis, K., et al., 2012. REE, Y, Nb, U, and Th Contents and Tetrad Effect in Zircon from a Magmatic-Hydrothermal F-Rich System of Sn-Rare Metal-Cryolite Mineralized Granites from the Pitinga Mine, Amazonia, Brazil. *Journal of South American Earth Sciences*, 33(1): 34–42. https://doi.org/10.1016/j.jsames.2011.07.004

Nash, W. P., Crecraft, H. R, 1985. Partition Coefficients for Trace Elements in Silicic Magmas. *Geochimica et Cosmochimica Acta*, 49(11): 2309–2322. https://doi.org/10.1016/0016-7037(85)90231-5

Neiva, A. M. R., Ramos, J. M. F, 2010. Geochemistry of Granitic Aplite-Pegmatite Sills and Petrogenetic Links with Granites, Guarda-Belmonte Area, Central Portugal. *European Journal of Mineralogy*, 22(6): 837–854. https://doi.org/10.1127/0935-1221/2010/0022-2072

Neiva, A. M. R., Silva, P. B., Ramos, J. M. F, 2012. Geochemistry of Granitic Aplite-Pegmatite Veins and Sills and Their Minerals from the Sabugal Area, Central Portugal. *Neues Jahrbuch Für Mineralogie-Abhandlungen*, 189(1): 49–74. https://doi.org/10.1127/0077-7757/2011/0209

Neiva, A. M. R., Gomes, M. E. P., Ramos, J. M. F., et al., 2008. Geochemistry of Granitic Aplite-Pegmatite Sills and Their Minerals from Arcozelo Da Serra Area (Gouveia, Central Portugal). *European Journal of Mineralogy*, 20(4): 465–485. https://doi.org/10.1127/0935-1221/2008/0020-1827

Neiva, J. M. C., 1944. Rochas Eruptivas da Península de Macau e das Ilhas de Taipa e Coloane. Boletim da Sociedade Geológica de Portugal, 3: 145–180

Pan, Y. M., 1997. Controls on the Fractionation of Isovalent Trace Elements in Magmatic and Aqueous Systems: Evidence from Y/Ho, Zr/Hf, and Lanthanide Tetrad Effect - a Discussion of the Article by M. Bau (1996). *Contributions to Mineralogy and Petrology*, 128(4): 405–408. https://doi.org/10.1007/s004100050317

Pan, Y. M., 1997. Controls on the Fractionation of Isovalent Trace Elements in Magmatic and Aqueous Systems: Evidence from Y/Ho, Zr/Hf, and Lanthanide Tetrad Effect—A Discussion of the Article by M. Bau (1996). *Contributions to Mineralogy and Petrology*, 128(4): 405–408. https://doi.org/10.1007/s004100050317

Pan, Y., Breaks, F.W., 1997. Rare-Earth Elements in Fluorapatite, Separation Lake Area, Ontario: Evidence for S-Type Granite-Rare-Element Pegmatite Linkage. *Canadian Mineralogist*, 35: 659–671

Peretyazhko, I. S., Savina, E. A, 2010. Tetrad Effects in the Rare Earth Element Patterns of Granitoid Rocks as an Indicator of Fluoride-Silicate Liquid Immiscibility in Magmatic Systems. *Petrology*, 18(5): 514–543. https://doi.org/10.1134/s086959111005005x

Qiu, Z. W., Yan, Q. H., Li, S. S., et al., 2017. Highly Fractionated Early Cretaceous I-Type Granites and Related Sn Polymetallic Mineralization in the Jinkeng Deposit, Eastern Guangdong, SE China: Constraints from Geochronology, Geochemistry, and Hf Isotopes. *Ore Geology Reviews*, 88: 718–738. https://doi.org/10.1016/j.oregeorev.2016.10.008

Quelhas, P., Dias, Á. A., Mata, J., et al., 2020. High-Precision Geochronology of Mesozoic Magmatism in Macao, Southeast China: Evidence for Multistage Granite Emplacement. *Geoscience Frontiers*, 11(1): 243–263. https://doi.org/10.1016/j.gsf.2019.04.011

Quelhas, P., Mata, J., Dias, Á. A, 2021. Evidence for Mixed Contribution of Mantle and Lower and Upper Crust to the Genesis of Jurassic I-Type Granites from Macao, SE China. *GSA Bulletin*, 133(1/2): 37–56. https://doi.org/10.1130/b35552.1

Ranjbar, S., Tabatabaei Manesh, S. M., Mackizadeh, M. A., et al., 2016. Geochemistry of Major and Rare Earth Elements in Garnet of the Kal-e Kafi Skarn, Anarak Area, Central Iran: Constraints on Processes in a Hydrothermal System. *Geochemistry International*, 54(5): 423–438. https://doi.org/10.1134/S0016702916050098

René, M., Stelling, J, 2007. Garnet-Bearing Granite from the Třebíč Pluton, Bohemian Massif (Czech Republic). *Mineralogy and Petrology*, 91(1/2): 55–69. https://doi.org/10.1007/s00710-007-0188-2

Ribeiro, M. L., Ramos, J. F., Pereira, E., et al., 2010. The Evolution of the Macao Geological Knowledge. *Geologia das Ex-Colónias da Ásia e Oceânia*, *Macau*, III: 259–266

Ribeiro, M. L., Ramos, J. M.., Pereira, E., et al., 1992. Notícia Explicativa da Carta Geológica de Macau na Escala 1/5 000. Serviços Geológicos de Portugal, 46.

Ríos Reyes, C.A., Alarcón, O.M.C., Takasu, A., 2009. A New Interpretation for the Garnet Zoning in Metapelitic Rocks of the Silgará Formation, Southwestern Santander Massif Colombia. *Earth Sciences Research Journal*, 12: 7–30

Scallion, K. L., Jamieson, R. A., Barr, S. M., et al., 2011. Texture and Composition of Garnet as a Guide to Contamination of Granitoid Plutons: An Example from the Governor Lake Area, Meguma Terrane, Nova Scotia. *The Canadian Mineralogist*, 49(2): 441–458. https://doi.org/10.3749/canmin.49.2.441

Sewell, R. J., Darbyshire, D. P. F., Langford, R. L., et al., 1992. Geochemistry and Rb-Sr Geochronology of Mesozoic Granites from Hong Kong. *Earth and Environmental Science Transactions of the Royal Society of Edinburgh*, 83(1/2): 269–280. https://doi.org/10.1017/s0263593300007951

Sewell, R. J., Campbell, S. D. G., Fletcher, C. J. N., et al., 2000. The Pre-Quaternary Geology of Hong Kong. Civil Engineering Department, Hong Kong SAR Government, Hong Kong

Shellnutt, J. G., Vaughan, M. W., Lee, H. Y., et al., 2020. Late Jurassic Leucogranites of Macao (SE China): a Record of Crustal Recycling during the Early Yanshanian Orogeny. *Frontiers in Earth Science*, 8: 1–24. https://doi.org/10.3389/feart.2020.00311

Simmons, W. B. S., Webber, K. L, 2008. Pegmatite Genesis: State of the Art. *European Journal of Mineralogy*, 20(4): 421–438. https://doi.org/10.1127/0935-1221/2008/0020-1833

Speer, J.A., Becker, S.W., 1992. Evolution of Magmatic and Subsolidus AFM Mineral Assemblages in Granitoid Rocks: Biotite, Muscovite, and Garnet in the Cuffytown Creek Pluton, South Carolina. *American Mineralogist*, 77: 821–833

Stevens, G., Villaros, A., Moyen, J. F, 2007. Selective Peritectic Garnet Entrainment as the Origin of Geochemical Diversity in S-Type Granites. *Geology*, 35(1): 9–12. https://doi.org/10.1130/g22959a.1

Streckeisen, A., le Maitre, R.W., 1979. A Chemical Approximation to the Modal QAPF Classification of the Igneous Rocks. *Neues Jahrbuch fur Mineralogie Abteilung*, 136: 169–206

Sun, S. S., McDonough, W. F, 1989. Chemical and Isotopic Systematics of Oceanic Basalts: Implications for Mantle Composition and Processes. *Geological Society, London, Special Publications*, 42(1): 313–345. https://doi.org/10.1144/gsl.sp.1989.042.01.19

Takahashi, Y., Yoshida, H., Sato, N., et al., 2002. W- and M-Type Tetrad Effects in REE Patterns for Water-Rock Systems in the Tono Uranium Deposit, Central Japan. *Chemical Geology*, 184(3/4): 311–335. https://doi.org/10.1016/s0009-2541(01)00388-6

Tao, J. H., Li, W. X., Li, X. H., et al., 2013. Petrogenesis of Early Yanshanian Highly Evolved Granites in the Longyuanba Area, Southern Jiangxi Province: Evidence from Zircon U-Pb Dating, Hf-O Isotope and Whole-Rock Geochemistry. *Science China Earth Sciences*, 56(6): 922–939. https://doi.org/10.1007/s11430-013-4593-6

Taylor, J., Stevens, G., 2010. Selective Entrainment of Peritectic Garnet into S-Type Granitic Magmas: Evidence from Archaean Mid-Crustal Anatectites. *Lithos*, 120(3/4): 277–292. https://doi.org/10.1016/j.lithos.2010.08.015

Tuttle, O. F., Bowen, N. L., 1958. Origin of Granite in the Light of Experimental Studies in the System $NaAlSi_3O_8$-$KAlSi_3O_8$-SiO_2-H_2O. *Geological Society of America Memoirs,* 74: 1–146. https://doi.org/10.1130/mem74

Veksler, I. V., Dorfman, A. M., Kamenetsky, M., et al., 2005. Partitioning of Lanthanides and Y between Immiscible Silicate and Fluoride Melts, Fluorite and Cryolite and the Origin of the Lanthanide Tetrad Effect in Igneous Rocks. *Geochimica et Cosmochimica Acta*, 69(11): 2847–2860. https://doi.org/10.1016/j.gca.2004.08.007

Villaros, A., Stevens, G., Buick, I. S, 2009. Tracking S-Type Granite from Source to Emplacement: Clues from Garnet in the Cape Granite Suite. *Lithos*, 112(3/4): 217–235. https://doi.org/10.1016/j.lithos.2009.02.011

Wang, Y. J., Fan, W. M., Zhang, G. W., et al., 2013. Phanerozoic Tectonics of the South China Block: Key Observations and Controversies. *Gondwana Research*, 23(4): 1273–1305. https://doi.org/10.1016/j.gr.2012.02.019

Whitworth, M. P, 1992. Petrogenetic Implications of Garnets Associated with Lithium Pegmatites from SE Ireland. *Mineralogical Magazine*, 56(382): 75–83. https://doi.org/10.1180/minmag.1992.056.382.10

Wu, C. Z., Liu, S. H., Gu, L. X., et al., 2011. Formation Mechanism of the Lanthanide Tetrad Effect for a Topaz- and Amazonite-Bearing Leucogranite Pluton in Eastern Xinjiang, NW China. *Journal of Asian Earth Sciences*, 42(5): 903–916. https://doi.org/10.1016/j.jseaes.2010.09.011

Wu, F. Y., Liu, X. C., Ji, W. Q., et al., 2017. Highly Fractionated Granites: Recognition and Research. *Science China Earth Sciences*, 60(7): 1201–1219. https://doi.org/10.1007/s11430-016-5139-1

Wu, F. Y., Sun, D. Y., Jahn, B. M., et al., 2004. A Jurassic Garnet-Bearing Granitic Pluton from NE China Showing Tetrad REE Patterns. *Journal of Asian Earth Sciences*, 23(5): 731–744. https://doi.org/10.1016/s1367-9120(03)00149-4

Xiang, Y. X., Yang, J. H., Chen, J. Y., et al., 2017. Petrogenesis of Lingshan Highly Fractionated Granites in the Southeast China: Implication for Nb-Ta Mineralization. *Ore Geology Reviews*, 89: 495–525. https://doi.org/10.1016/j.oregeorev.2017.06.029

Xu, B., Jiang, S. Y., Wang, R., et al., 2015. Late Cretaceous Granites from the Giant Dulong Sn-Polymetallic Ore District in Yunnan Province, South China: Geochronology, Geochemistry, Mineral Chemistry and Nd–Hf Isotopic Compositions. *Lithos*, 218/219: 54–72. https://doi.org/10.1016/j.lithos.2015.01.004

Yang, J. B., Zhao, Z. D., Hou, Q. Y., et al., 2018. Petrogenesis of Cretaceous (133–84 Ma) Intermediate Dykes and Host Granites in Southeastern China: Implications for Lithospheric Extension, Continental Crustal Growth, and Geodynamics of Palaeo-Pacific Subduction. *Lithos*, 296/297/298/299: 195–211. https://doi.org/10.1016/j.lithos.2017.10.022

Yang, Y. L., Ni, P., Yan, J., et al., 2017. Early to Late Yanshanian I-Type Granites in Fujian Province, SE China: Implications for the Tectonic Setting and Mo Mineralization. *Journal of Asian Earth Sciences*, 137:

194–219. https://doi.org/10.1016/j.jseaes.2016.11.017

Yardley, B. W. D., 1977. An Empirical Study of Diffusion in Garnet. *American Mineralogist*, 62: 793–800

Ye, M. F., Li, X. H., Li, W. X., et al., 2007. SHRIMP Zircon U-Pb Geochronological and Whole-Rock Geochemical Evidence for an Early Neoproterozoic Sibaoan Magmatic Arc along the Southeastern Margin of the Yangtze Block. *Gondwana Research*, 12(1/2): 144–156. https://doi.org/10.1016/j.gr.2006.09.001

Yurimoto, H., Duke, E. F., Papike, J. J., et al., 1990. Are Discontinuous Chondrite-Normalized REE Patterns in Pegmatitic Granite Systems the Results of Monazite Fractionation? *Geochimica et Cosmochimica Acta*, 54(7): 2141–2145. https://doi.org/10.1016/0016-7037(90)90277-r

Zajacz, Z., Halter, W. E., Pettke, T., et al., 2008. Determination of Fluid/Melt Partition Coefficients by LA-ICPMS Analysis of Co-Existing Fluid and Silicate Melt Inclusions: Controls on Element Partitioning. *Geochimica et Cosmochimica Acta*, 72(8): 2169–2197. https://doi.org/10.1016/j.gca.2008.01.034

Zaraisky, G. P., Aksyuk, A. M., Devyatova, V. N., et al., 2009. The Zr/Hf Ratio as a Fractionation Indicator of Rare-Metal Granites. *Petrology*, 17(1): 25–45. https://doi.org/10.1134/S0869591109010020

Zhang, Y., Yang, J. H., Chen, J. Y., et al., 2017. Petrogenesis of Jurassic Tungsten-Bearing Granites in the Nanling Range, South China: Evidence from Whole-Rock Geochemistry and Zircon U-Pb and Hf-O Isotopes. *Lithos*, 278/279/280/281: 166–180. https://doi.org/10.1016/j.lithos.2017.01.018

Zhang, Y., Yang, J. H., Sun, J. F., et al., 2015. Petrogenesis of Jurassic Fractionated I-Type Granites in Southeast China: Constraints from Whole-Rock Geochemical and Zircon U-Pb and Hf-O Isotopes. *Journal of Asian Earth Sciences*, 111: 268–283. https://doi.org/10.1016/j.jseaes.2015.07.009

Zhao, J. X., Cooper, J. A, 1993. Fractionation of Monazite in the Development of V-Shaped REE Patterns in Leucogranite Systems: Evidence from a Muscovite Leucogranite Body in Central Australia. *Lithos*, 30(1): 23–32. https://doi.org/10.1016/0024-4937(93)90003-u

Zhao, Z. H., Xiong, X. L., Han, X. D., et al., 2002. Controls on the REE Tetrad Effect in Granites: Evidence from the Qianlishan and Baerzhe Granites, China. *Geochemical Journal*, 36(6): 527–543. https://doi.org/10.2343/geochemj.36.527

Zhou, X. M., Li, W. X, 2000. Origin of Late Mesozoic Igneous Rocks in Southeastern China: Implications for Lithosphere Subduction and Underplating of Mafic Magmas. *Tectonophysics*, 326(3/4): 269–287. https://doi.org/10.1016/s0040-1951(00)00120-7

Zhou, X. M., Sun, T., Shen, W. Z., et al., 2006. Petrogenesis of Mesozoic Granitoids and Volcanic Rocks in South China: a Response to Tectonic Evolution. *Episodes*, 29(1): 26–33. https://doi.org/10.18814/epiiugs/2006/v29i1/004

Zhou, Z. M., Ma, C. Q., Xie, C. F., et al., 2016. Genesis of Highly Fractionated I-Type Granites from Fengshun Complex: Implications to Tectonic Evolutions of South China. *Journal of Earth Science*, 27(3): 444–460. https://doi.org/10.1007/s12583-016-0677-3